Clays and Clay Minerals, Vol. 68, No. 6:553–579, 2020

GENESIS OF THE YARIKÇI HYDROTHERMAL CLAY DEPOSIT WITHIN THE MESOZOIC METAMORPHIC UNITS, MİHALIÇÇIK, ESKİŞEHİR, TURKEY

Selahattin Kadir[1] *, Hülya Erkoyun[1], and Tacit Külah[2]

[1]Department of Geological Engineering, Eskişehir Osmangazi University, TR-26480 Eskişehir, Turkey
[2]Department of Geological Engineering, Kütahya Dumlupınar University, TR-43100 Kütahya, Turkey

Abstract—Hydrothermal alteration led to development of the Yarıkçı clay deposit within the Mesozoic chlorite-, muscovite-, chlorite-muscovite-schist, and garnet-graphite phyllite units along NW–SE- and N–S-trending faults in Mihalıççık in western central Anatolia. The geological, mineralogical, and geochemical characteristics and genesis of this economically important clay deposit have not been examined in detail previously. The present study has attempted to fill this gap. Green smectitic and cream kaolinitic claystones are abundant with smaller amounts of gray illite, dark brown Fe oxides, and silica phases occurring as stockwork/fracture infill and stain/coating. These units are covered by a dark, hard, sharp-edged, and thick silica cap. Metamorphic units exhibit cataclastic texture due to tectonic activities. Muscovite is mostly degraded to kaolinite, and feldspars show sericitization and argillization. Kaolinite typically has a platy form with irregular margins and locally sub-rounded, book-like texture suggesting hydrolysis during the hydrothermal injections. The association of Fe oxides, cristobalite/tridymite/quartz, gypsum/anhydrite, and jarosite are indicative of intense hydrothermal activities and development of kaolinite under acidic geochemical conditions. The local enrichment of SiO_2, Fe_2O_3, S, Cu, and Au also supports this suggestion. The leaching of Sr, Rb, Ba, and Zr, and the slight increase in LREE/MREE+HREE ratios together with the negative Eu and Ce anomalies suggest the selective dissolution of muscovite, garnet, feldspar, and pyroxene by the hydrothermal fluids. Thus, abundant claystones of smectite and kaolinite were formed via the increase in Al+Fe+Mg/Si and Al±Fe/Si ratios in the alkaline and acidic environment, respectively, under the tectonic control of hydrothermal activity as seen in the alteration of chlorite, muscovite, and feldspar in metamorphic units.

Keywords—Eskişehir · Genesis · Geochemistry · Hydrothermal clay deposit · Mineralogy · Mesozoic metamorphism · Turkey

INTRODUCTION

The development of kaolinization as a result of tectonically controlled hydrothermal alteration of metamorphic units is rare in Anatolia (Kadir and Akbulut 2009; Sayın 2016). In contrast, kaolinite deposits in Anatolia are formed mostly by hydrothermal alteration of acidic or intermediate volcanic rocks (Seyhan 1978; Sayın 2007; Ece and Schroeder 2007; Ece et al. 2008; Erkoyun and Kadir 2011; Kadir et al. 2011, 2014).

The Yarıkçı clay deposit formed along the tectonically controlled hydrothermal alteration of Mesozoic metamorphic units (Fig. 1). The Yarıkçı clay deposit has been mined since the 1990s to provide raw material for the production of tile and glaze. The Yarıkçı clay deposit and the surrounding kaolinite deposits in the Mihalıççık region have 1,000,000 tons of minable (inferred) reserves, and 3,330,380 tons of inferred + probable reserves (8th Five-Year Development Plan – State Planning Organization of Turkey 2001). Smectite and kaolinite in the Yarıkçı clay deposit were formed by hydrothermal alteration of crystal tuff (Fujii et al. 1995). Ömeroğlu Sayıt et al. (2018) studied the hydrothermal kaolinite deposit within Mesozoic granitic intrusions in the Ahırözü (Mihalıççık) area and reported that the kaolinization had developed under the influence of a low-sulfidation system showing argillization. The Taşoluk (Afyonkarahisar, western Anatolia) kaolinite formed in association with illite in Paleozoic chlorite and sericitic mica schists via a dissolution and precipitation mechanism during a hydrothermal alteration process (Kadir and Akbulut 2009).

Due to the lack of detailed studies of the lithological, mineralogical, micromorphological, and geochemical characteristics, the genesis of the Yarıkçı clay deposit, which consists of smectite associated with kaolinite and illite within Mesozoic metamorphic units, is open to debate. The present study aimed to determine the formation and association of smectite with both kaolinite and illite and their lateral and vertical distributions in the Mihalıççık region. The present study suggested that these clay deposits originated from the hydrothermal alteration of Mesozoic metamorphic units and the physicochemical conditions, which have not been discussed previously. The results of this research will provide information and a useful tool in the study of similar hydrothermal alteration sources of raw materials in western Anatolia.

GEOLOGICAL SETTING AND DESCRIPTION OF CLAY DEPOSIT

The parent rocks of the Yarıkçı clay deposit consist of the Mesozoic Mihalıççık metamorphic units composed of chlorite schist, glaucophane schist, glaucophane-chlorite schist, muscovite schist, chlorite-muscovite schist, and garnet-graphite phyllite (Figs. 1, 2, and 4a,b). This unit represents a transition from greenschist to blueschist facies (Davis and Whitney 2006; Kadir and Erkoyun 2015).

The metamorphic units also include quartzite layers and accessory mica minerals (Kulaksız 1981; Yılmaz 1981; Gözler

* E-mail address of corresponding author: skadir.icc@gmail.com
DOI: 10.1007/s42860-020-00097-3

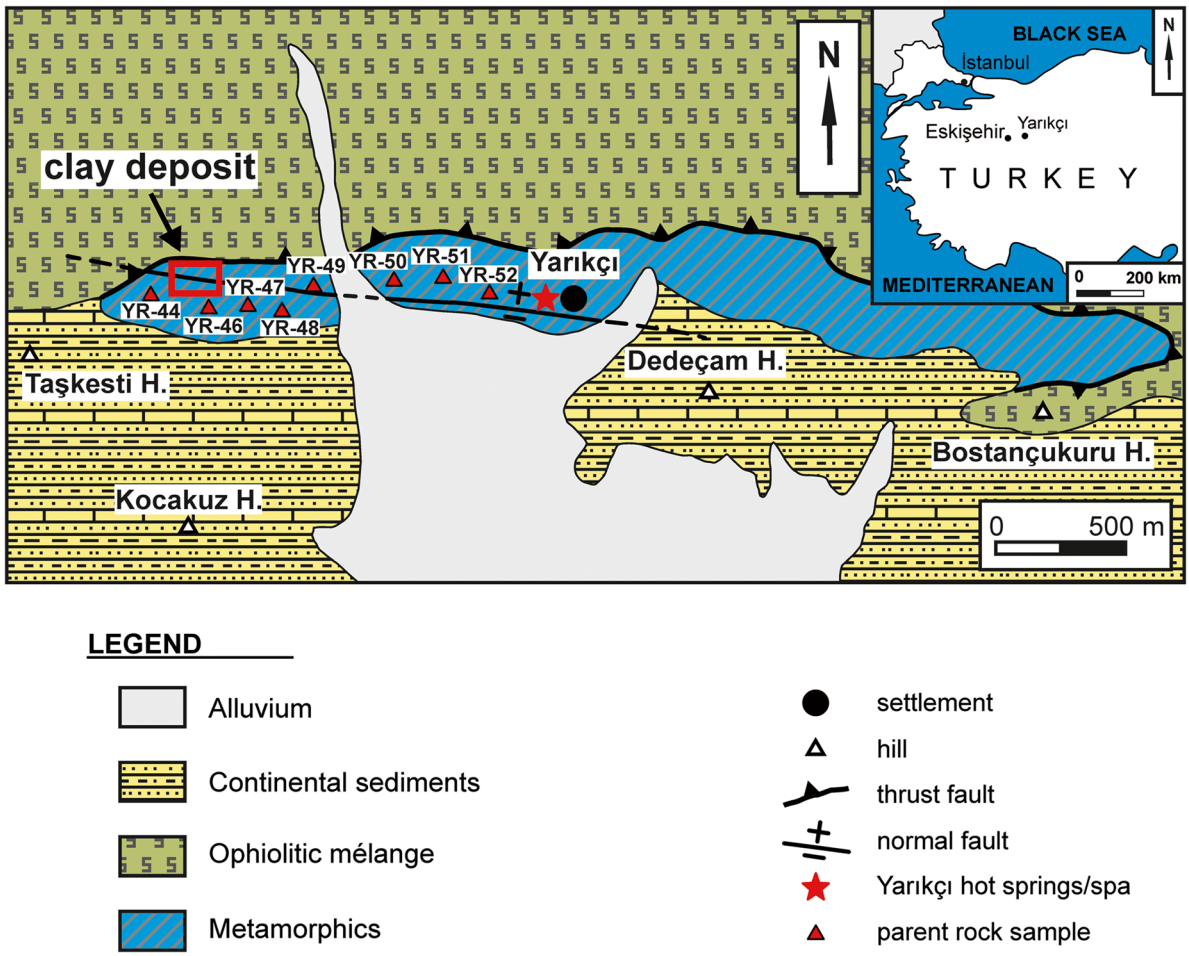

Fig. 1. Geological map of the study area (modified after Koçak 1975) and locations of the parent rock samples (see Fig. 3 for locations of the altered samples)

et al. 1996; Akbulut et al. 2006) and they are overthrust by an Upper Cretaceous ophiolitic mélange composed of serpentinized ultramafics, peridotite, and radiolarite units (Şengör and Yılmaz 1981; Okay 1989; Okay et al. 2001). Neogene continental clastics, volcanics, volcaniclastics, and lacustrine carbonates overlie these units unconformably (Boyraz 2004; Karakaş et al. 2007; Kadir et al. 2017). All the aforementioned formations are overlain unconformably by Quaternary alluvium (Fig. 2).

Structural features indicate that the Eskişehir region is affected by major and minor E–W-trending faults that have been under the control of the tectonic influence of the North Anatolian Fault Zone since the Miocene (Şengör et al. 1985). These Cretaceous–Tertiary tectonic activities and E–W-trending Yarıkçı fault zone are associated with sulfur-bearing Yarıkçı hot springs and spa (Seyhan 1968; Koçak 1975). The faults in this zone are the main reason for the deformation of the metamorphic units and formation of the clay deposits during and following hydrothermal alteration (Seyhan 1968).

Hydrothermal alteration developed within the metamorphic units along NW–SE-trending main and N–S-trending secondary normal faults (Figs. 3 and 4c–e). Enrichment of smectite, kaolinite, illite, silica, and iron phases caused the development of several mineral associations recognizable by the color of claystone outcrops within the clay deposit (Figs. 3 and 4f). Generally, kaolinite is identified by cream-colored outcrops in the southern part of the deposit. Kaolinite mostly includes silica-filling veins and subvertical fractures, and staining by Fe oxides (Figs. 3 and 4g–i). Kaolinitic claystones are also accompanied by irregular green smectitic units (Fig. 4j). Smectitic claystone is abundant in the deposit and mostly encloses Fe oxide-rich fracture in-fills (Figs. 3 and 4k). Smectitic claystone is accompanied by brownish-red, Fe oxide-rich phases along the fault zones (Figs. 3 and 4l,m). Goethite/hematite-type Fe oxides are mostly associated with kaolinite-bearing smectitic claystones. The gray, plastic, and locally friable claystones composed mainly of illite are the outcrops of the clay deposit (Figs. 3 and 4n). The northwestern part of the clay deposit is overlain by a dark-gray, hard, and sharp-edged silica cap (Figs. 3 and 4o).

https://doi.org/10.1007/s42860-020-00097-3 Published online by Cambridge University Press

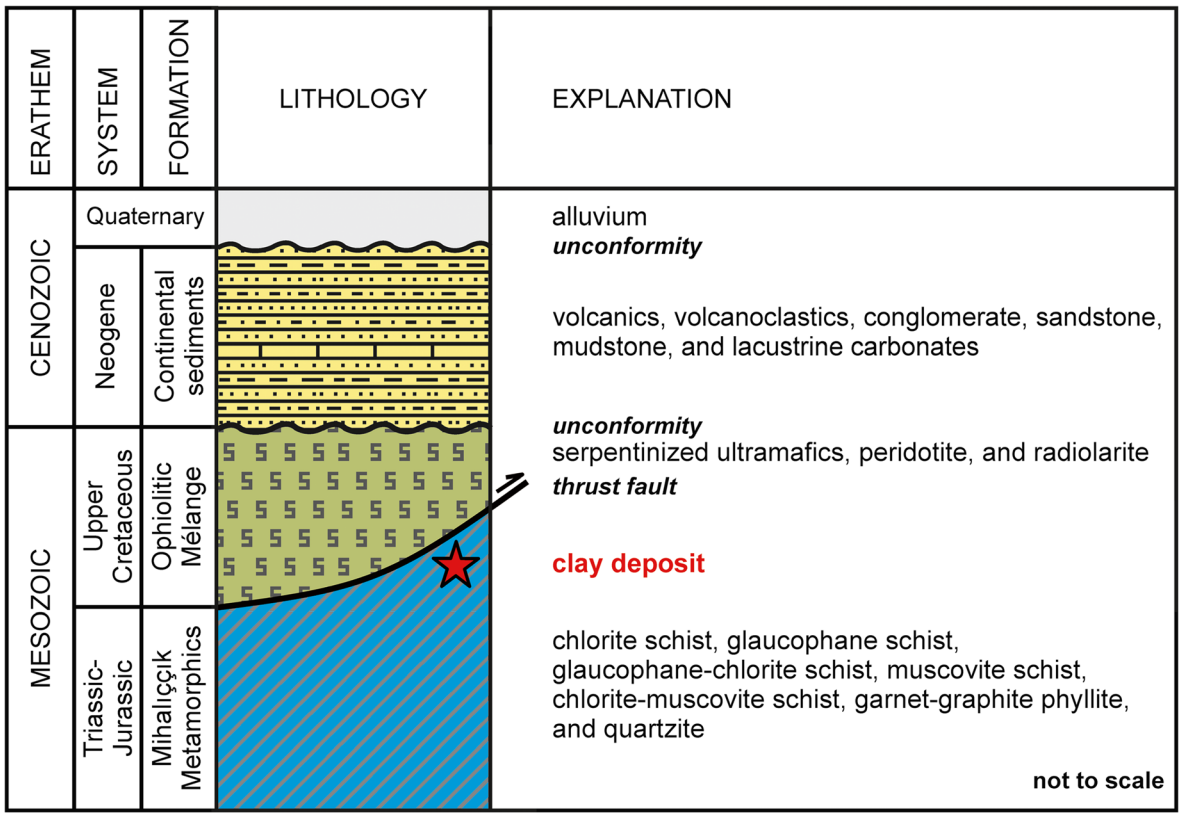

Fig. 2. Generalized stratigraphic column of the study area (simplified from Kadir et al. 2017)

MATERIALS AND METHODS

Eight representative, fresh schists and 44 claystone samples were collected based on the lithologies and colors of the Yarıkçı clay deposit and the parent rocks of the metamorphic units located along lateral and vertical variations (Figs. 1 and 3). Thin sections of fresh schist were examined under a Nikon-LV 100Pol (Nikon Corporation, Tokyo, Japan) polarizing microscope. Samples selected to represent various degrees of alteration and related colors were crushed manually and powdered using a tungsten carbide pulveriser for X-ray diffraction (XRD) and geochemical analyses.

The separation of the clay fraction was undertaken following the removal of Fe(III) oxide and/or hydroxide cements by the sodium dithionite-citrate procedure and 30% H_2O_2 was used to eliminate organic matter (Kunze and Dixon 1986). The treated and dried (<105°C temperature) samples were sieved to <2 mm. 100 g of the <2 mm fraction was mixed with deionized water and disaggregated using a 'Stir-Pak' (Cole-Parmer, Vernon Hills, Illinois, USA) mixer head and mixer controller to obtain clay fractions of these samples. The <2 μm fractions were separated from the silt (2–50 μm) by using repeated siphoning of the dispersed material. The clay fraction was separated by sedimentation of the suspension after 24 h of dispersion in distilled water and removal of the upper 5 cm, followed by centrifugation for 10 min at 2451×*g* (4000 rpm) using a Hettich 32A centrifuge (Andreas Hettich GmbH and Co. KG, Tuttlingen, Germany).

Several oriented mounts were prepared from each clay fraction by dropping a small amount of clay suspension onto a glass slide and drying in air. One oriented mount was solvated using ethylene glycol vapor at 60°C for 2 h to expand and identify clay minerals. Other oriented mounts were heated at 350 and at 550°C for 2 h to assist in differentiating chlorite from kaolinite.

The mineralogical characteristics of the samples were determined using powder XRD (Rigaku D/Max–2200, Ultima PC, Tokyo, Japan). The bulk powders and clay mounts prepared using the method mentioned above were scanned using CuKα radiation (40 kV and 30 mA) with a 1° divergence slit, a 0.15° anti-scatter slit, and a 1° receiving slit. A 0.30 mm monochromator receiving slit and a graphite monochromator were used to filter out all but CuKα radiation. The samples were scanned at a speed of 1°2θ/min. Randomly oriented mounts of powdered samples were scanned to determine the mineralogy. Semi-quantitative abundances of rock-forming minerals were determined using sharp and unambiguous reflection intensities on the XRD patterns (Brindley 1980). The clay mineral relative abundances were determined from basal reflections and the mineral intensity factors of Moore and Reynolds (1989).

Scanning electron microscopy–energy dispersive X-ray analysis (SEM-EDX) studies were performed at Middle East Technical University (Turkey) and Eskişehir Osmangazi University (Turkey) using a QUANTA 400F Field Emission SEM

https://doi.org/10.1007/s42860-020-00097-3 Published online by Cambridge University Press

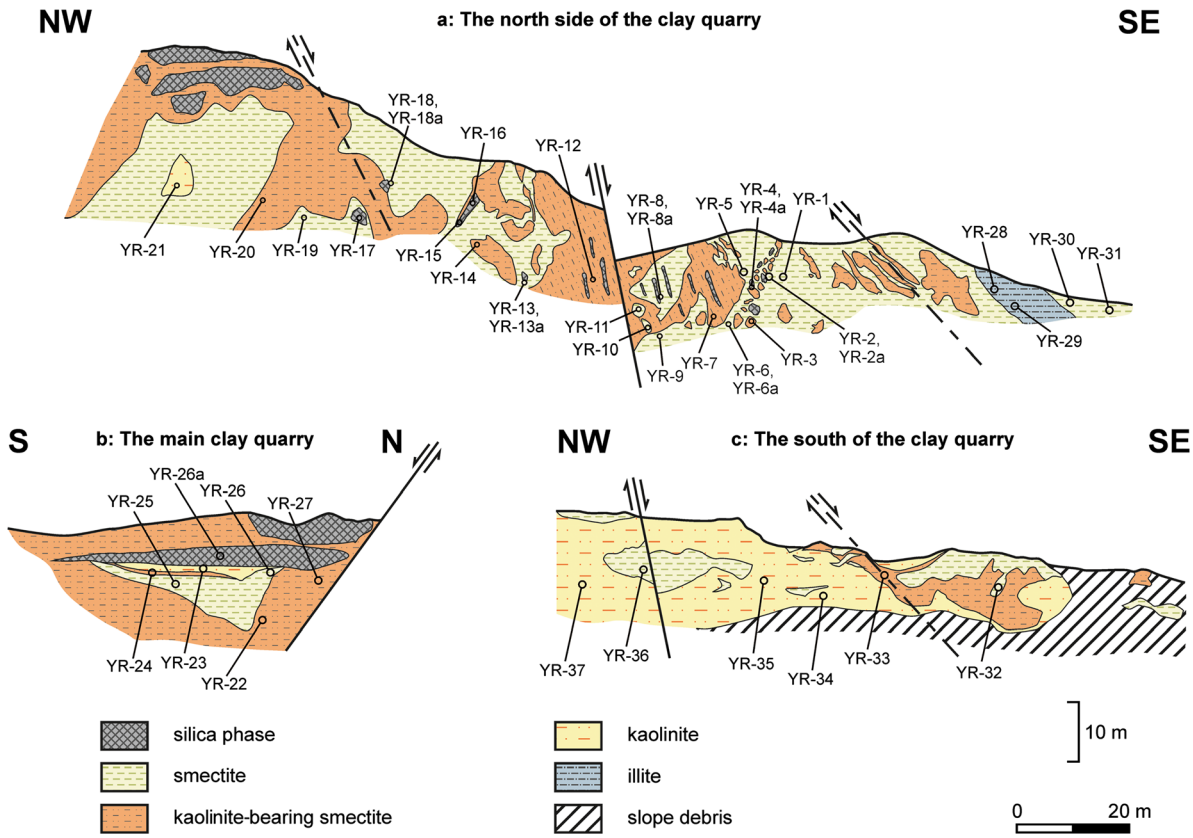

Fig. 3. Profiles of the Yarıkçı clay deposit

instrument (Thermo Fisher Scientific, Hillsboro, Oregon, USA) and an Hitachi-Regulus 8230 and Oxford instrument ULTRIM EXTREME detector, respectively. The bulk specimens that consisted predominantly of clay were prepared for SEM-EDX analysis by sticking the freshly broken surface of each rock sample onto an aluminum sample holder using double-sided tape. The samples were then coated with a thin film (~3 nm) of gold/palladium using a Polaron range sputter coater (Quorum Technologies Ltd., Ashford, Kent, UK).

Nine representative claystone samples, seven silica-phase samples from the clay deposit, and six metamorphic rock samples from the parent rocks were analyzed for major and trace elements at the Bureau Veritas Mineral Laboratories (Vancouver, Canada) using a Perkin Elmer Elan 9000 (PerkinElmer, Inc., Waltham, Massachusetts, USA) inductively coupled plasma–atomic emission spectrometer (ICP-AES) and mass spectrometer (ICP-MS) and a Spectro (Spectro Analytical Instruments Inc., Mahwah, New Jersey, USA) XLAB-2000 PEDX-ray fluorescence spectrometer (PEDXRF), which was calibrated using USGS interlaboratory standards. The ICP-AES and ICP-MS analyses were carried out on lithium metaborate/tetraborate fused samples after dissolution in dilute nitric acid. Loss on ignition (LOI) values were determined from the mass differences before and after ignition at 1000°C. Total Fe was reported as Fe_2O_3 and total C was determined by ignition followed by measurement using an infrared spectrometric cell in a LECO Carbon Analyzer (LECO Corporation, St. Joseph, Michigan, USA); the latter analyses were carried out at the Bureau Veritas, Vancouver, Canada.

The detection limits for the chemical analyses were 0.01 wt.% for most major element oxides, but were 0.002 wt.% for Cr_2O_3, 0.04 wt.% for Fe_2O_3, 0.02 wt.% for total C and total S, 0.1 wt.% for LOI, and between 0.01 and 1 mg/kg for almost all trace elements. Samples were analyzed in duplicate and the accuracy and analytical precision of the major element measurements were assessed by analyzing the standard reference materials STD SO-18, STD SO-19, STD GS311-1, and STD GS910-4 for major elements and by analyzing the standard reference materials STD SO-18, STD SO-19, STD DS10, and STD OREAS45EA for trace elements.

The degree of chemical index of weathering (CIW) of claystone, silica phase, and metamorphic parent whole-rock samples was calculated using the following equation (Harnois 1988):

$$CIW = [Al_2O_3/(Al_2O_3 + CaO^* + Na_2O)] \times 100$$

$$CaO^* = \text{The amount of CaO incorporated into the silicate fraction.}$$

Fresh metamorphic rock samples composed of chlorite schist, muscovite schist, chlorite-muscovite schist, and garnet-graphite phyllite representing the parent rocks of the clay deposit and claystone samples were used for mass gain

https://doi.org/10.1007/s42860-020-00097-3 Published online by Cambridge University Press

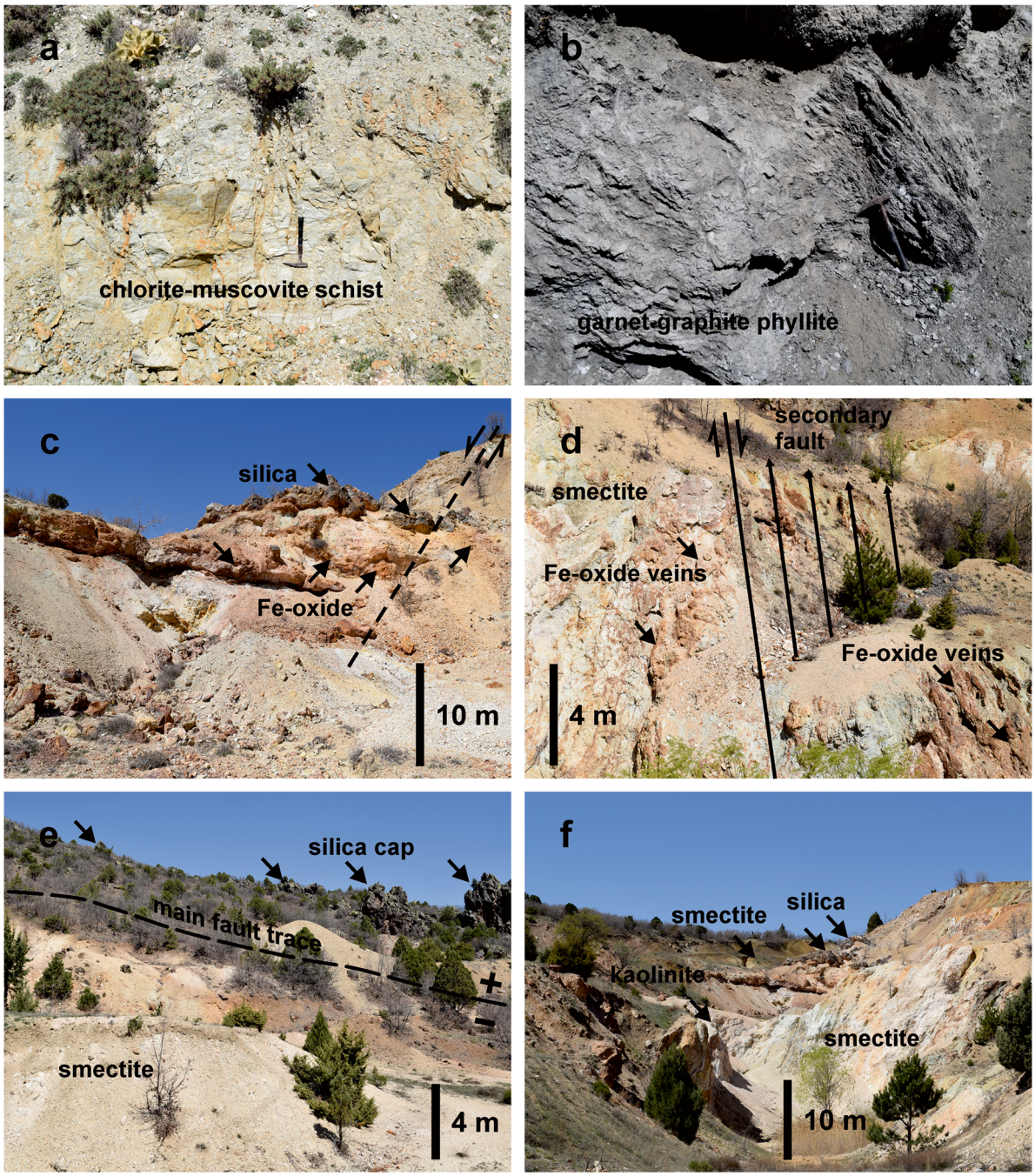

Fig. 4. Field view of: **a** chlorite-muscovite schist; **b** garnet-graphite phyllite; **c** Yarıkçı clay deposit and covered/enclosed silica cap and phases along the main fault; **d** secondary fault in the northern site of the deposit; **e** main fault and associated silica caps in the northern site of the deposit; **f** relationship of smectite and kaolinite abundant claystones with silica phase; **g–i** subvertical Fe oxide and silica veins in the kaolinitic claystone; **j** relationship of the kaolinite and smectite in claystone; **k** Fe-oxide veins and stains in smectite-rich claystone; **l**, **m** Fe oxides in smectitic claystone; **n** illitic claystone; **o** silica cap at the top of the deposit

and loss calculation. Mass gains and losses have been calculated and estimated by using the *EASYGRESGRANT* program (Eq. 1) (López-Moro 2012) and from plots of the geochemical analyses on isocon diagrams (Grant 1986, 2005).

$$C_i^A = \left(M^O/M^A\right)C_i^O \quad (1)$$

where C_i is the concentration of component i, O indicates the fresh rock, and A indicates the altered rock. The M^O and M^A values are the masses (as wt.% for major oxide or ppm for trace

https://doi.org/10.1007/s42860-020-00097-3 Published online by Cambridge University Press

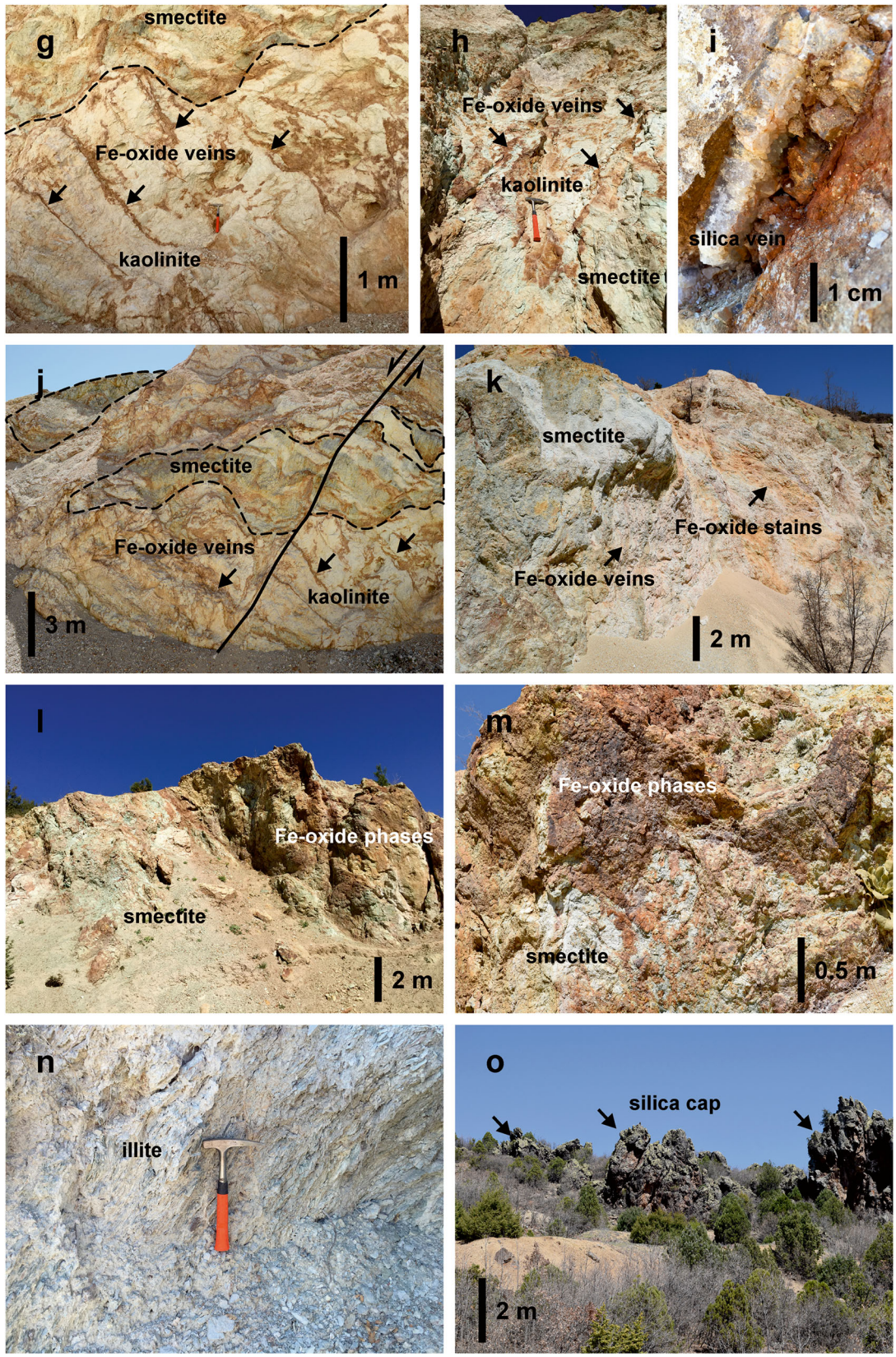

Fig. 4 (continued)

https://doi.org/10.1007/s42860-020-00097-3 Published online by Cambridge University Press

and rare earth elements) of the fresh and altered rocks, respectively.

The C_i^A/C_i^O ratios were plotted to obtain the slopes of the isocon graphic lines from the fresh and the altered rock analytical data using Eq. 2.

$$\Delta C_i/C_i^O = \left(M^A/M^O\right)\left(C_i^A/C_i^O\right)-1 \quad (2)$$

where ΔC_i is the gain or loss of mass. Based on clusters of slopes, components with slope values close to 1.00 were assumed to be immobile.

Finally, the mass change of a component is calculated by applying Eq. 3.

$$\Delta C_i^A/C_i^O = \left(C_i^A/C_i^O\right)-1 \quad (3)$$

The sample compositions that plot above the isocon line indicate a gain during the alteration process and samples that plot below this line represent a loss during alteration.

RESULTS

Petrography

The parent rocks of the Yarıkçı clay deposit are represented by lepidoblastic and cataclastic chlorite schist, chlorite-muscovite schist, muscovite schist, and blastoporphyritic garnet-graphite phyllite, which is composed of chlorite, muscovite, sericite, graphite, garnet, quartz, and calcite, and accessory pyroxene (Figs. 4a,b and 5). Fe-(oxyhydr)oxides developed along the foliation of the schist (Fig. 5a,b). The partially or completely altered muscovite and degraded quartz crystals exhibit cataclastic character such as bending and disaggregation, and plagioclase (albite) and K-feldspar are mostly argillized and sericitized (Fig. 5a–f). Carbonitization is widespread in chlorite-muscovite schist samples (Fig. 5c). Accessory garnet and abundant graphite, quartz, and sericite occur in garnet-graphite phyllite (Fig. 5g,h).

XRD determinations

The XRD analyses of the bulk samples and clay-mineral fractions collected from the Yarıkçı clay deposit are given in Table 1 and Fig. 6. The mineralogical composition shows a heterogeneous distribution. Kaolinite was determined by diagnostic sharp basal reflections at 7.14–7.17 Å and 3.57–3.58 Å, and non-basal less intense reflections of triplets and doublets at 4.46–4.47, 4.34–4.37, 4.18–4.19; 2.56–5.57, 2.52–2.49, 2.34, and 2.29 Å, showing clearly a highly crystallized kaolinite (Brindley 1980; Wilson 1987) (Fig. 6). The spacing of the basal reflection of kaolinite was not affected by ethylene-glycol saturation, but its intensity decreased and then collapsed due to dehydroxylation following heating at 350°C and 550°C (for 2 h), respectively (Fig. 6, YR-21). Smectite was determined by narrow, sharp basal reflections at 14.10–15.01 Å and the spacing of the basal reflection of smectite in sample YR-9 was expanded to 17.14 Å with ethylene-glycol treatment and progressively decreased to 10.04 and 9.81 Å following heating at 350°C and 550°C for 2 h, respectively (Fig. 6). The d_{060} value of 1.49 Å indicates dioctahedral smectite (Moore and Reynolds 1989). Illite was also determined by basal reflections of 10.00–9.99 Å and 5.00–4.99 Å that were not affected by ethylene-glycol treatment and heating at 350°C and 550°C (Fig. 6, YR-28). Chlorite in the parent schist rock (samples YR-34, YR-44, YR-48, and YR-52) was determined by sharp diagnostic reflections at 14.17–14.10, 7.07, and 3.54 Å. The basal reflection of chlorite at 14.17 Å was not affected by ethylene-glycol treatment. The intensity of this peak was unchanged at 350°C but slightly reduced at 550°C (Fig. 6, YR-44). Cristobalite, tridymite, and a small amount of quartz are present in altered units and with more present in the silica cap and fracture/fault infill and determined by reflections at 4.05 Å, 4.11 Å, and 3.34, 4.26 Å, respectively (Fig. 6, YR-13 and YR-20).

Kaolinite is abundant in the cream-colored claystone. Smectite and smectite associated with small amounts of kaolinite is abundant in the irregular-form green and brownish-red claystone units which are prevalent in the deposit. Smectite is associated mostly with cristobalite/tridymite in kaolinite and rarely in smectite-abundant claystone. Generally, kaolinite shows positive correlation with goethite/hematite in the claystones. Illite is abundant in the gray claystone at the margin of the deposit and is associated with small amounts of smectite, kaolinite, and quartz. Parent rocks of the claystones are composed mainly of chlorite associated with illite/muscovite, quartz, and accessory kaolinite, feldspar, and pyroxene (Table 1).

SEM-EDX determinations

Observations by SEM indicate that irregular kaolinite plates developed on or bordered altered, book-like muscovite crystals (Fig. 7a,b). The EDX spectra of muscovite plates show strong peaks for Si, Al, and K (Fig. 8a). Kaolinite in claystone occurs in a condensed, irregular platy form and is occasionally found in hexagonal form (Fig. 7c). The EDX spectra of kaolinite plates show strong peaks of Si and Al (Fig. 8b) along with local kaolinite exhibiting sub-rounded book-like morphologies (Fig. 7d). Chlorite shows irregular plates and rosette patterns (Fig. 7e). The EDX spectra of chlorite have signals of Si, Al, Mg, Fe, and weakly of K (Fig. 8c). Smectite in claystone exhibits a flaky form (Fig. 7f). Flaky smectite is characterized by strong EDX spectra and signals of Si, Al, Mg, and of poor Fe and Na (Fig. 8d).

Kaolinite and smectite are also associated with abundant sub-rounded disc-shaped forms resembling hematite, as determined by the strong Fe peak associated with faint Si, Al, and S spectra which originated from the surrounding kaolinite and accessory jarosite crystals (Figs. 7g–k and 8e). Rod- and locally star-like goethite also formed as a thin film on the surface of siliceous materials yielding a strong Si peak, which is diagnostic of opaline (Figs. 7i–k and 8f).

Subhedral jarosite also coexists with clayey materials (Fig. 7l). Gypsum/anhydrite occurs as condensed, irregular, rod-shaped structures that are identified by the strong S and Ca peaks, associated with poor Al and Si peaks, possibly belonging to the surrounding kaolinite (Figs. 7m,n and 8g).

https://doi.org/10.1007/s42860-020-00097-3 Published online by Cambridge University Press

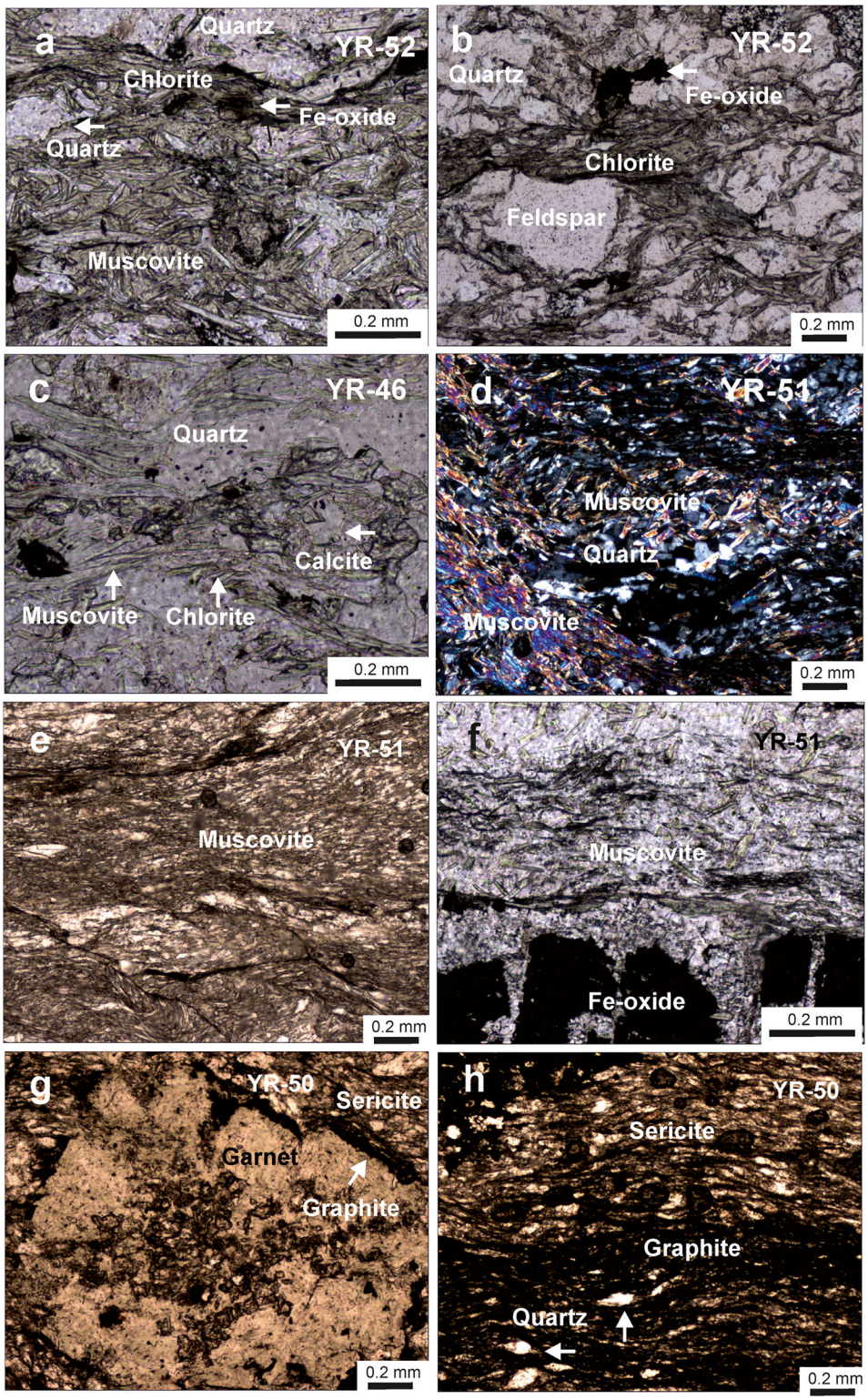

Fig. 5. Photomicrographs of: **a**–**b** chlorite cementing muscovite, feldspar, and quartz crystals; plain-polarized light (YR-52); **c** calcite crystal associated with muscovite, quartz, and chlorite crystal; plain-polarized light (YR-46); **d** muscovite associated with quartz showing cataclastic texture; crossed nicols light (YR-51); **e**, **f** subparallel muscovite crystal with Fe oxide in muscovite schist; plain-polarized light (YR-51); **g** euhedral coarse-grained garnet surrounded by graphite in sericite schist; plain-polarized light (YR-50); and **h** subparallel orientation of graphite with sericite enclosing quartz crystal; plain-polarized light (YR-50)

https://doi.org/10.1007/s42860-020-00097-3 Published online by Cambridge University Press

Table 1. Mineralogical variations in the Yarıkçı clay deposit

Sample	Rock type	Sme	Kln	Ilt/Ms	Chl	Gth/Hem	Jrs	Crs/Trd	Qz	Fsp	Px
Parent rock											
YR-44	chlorite schist		+	+	+				+	acc	acc
YR-48	chlorite schist		acc	++	++				+	acc	acc
YR-52	chlorite schist			++	++				+	+	+
Claystone											
YR-1	Claystone	++++	+	acc				acc	acc		
YR-2	silicified claystone	+++	acc					++	+		
YR-4	silicified claystone	+++		acc				++	acc		
YR-5	Claystone	++	++					+			
YR-6	silicified claystone	+++		acc				+	acc		
YR-8	Claystone	++++	acc	+			acc		acc		
YR-9	Claystone	++++	acc	acc				+			
YR-10	silicified claystone	+++	acc					++			
YR-13	Claystone	++						++	+		
YR-14	Claystone	++++	+	acc		acc		acc			
YR-18	Claystone	+++					acc	++			
YR-25	Claystone	++++	acc					+			
YR-26	Claystone	+++						++			
YR-31	silicified claystone	++	acc					++	+		
YR-32	silicified claystone	++						+++			
YR-36	silicified claystone	++						+++			
YR-3	Fe-rich claystone	++		acc		++		++	acc		
YR-7	Fe-rich claystone	++		acc		+++					
YR-12	Claystone	+++	+			+		acc	+		
YR-20	Claystone	++	++	acc		+		+	acc		
YR-21	Claystone	+	++++				acc				
YR-22	Claystone	++	++			+	acc	+			
YR-23	Claystone	+	+++			acc	acc	+			
YR-24	Fe-rich claystone	++	++			++		acc	acc	acc	
YR-27	Claystone	++	+++			acc					
YR-28	Claystone	+	+	++		acc			+		
YR-29	Claystone	acc	+	+					++	acc	
YR-33	Claystone	++	++			+		acc			
YR-34	Claystone	+	+++	+		acc			acc		
YR-35	Claystone	++	+++			acc					
YR-37	Claystone	+	++++			acc			acc		
YR-38	Claystone	+	+++	acc		+					
Silica phase											
YR-15	silica phase							+++++			
YR-16	silica phase					acc			+++++		
YR-17	silica phase	acc	acc	acc		acc		+++	++	acc	

Sme: smectite; Kln: kaolinite; Ilt/Ms: illite/muscovite; Chl: chlorite; Gth/Hem: goethite/hematite; Jrs: jarosite; Crs/Trd: cristobalite/tridymite; Qz: quartz; Fsp: feldspar; Px: pyroxene; acc: accessory; +: relative abundance of mineral (mineral-name abbreviations after Whitney and Evans 2010)

Geochemistry

Chemical analyses (Table 2) revealed that the parent rock and claystone samples are characterized by SiO_2 (avg. 56.44 and 51.71 wt.%, respectively), Al_2O_3 (avg. 15.36 and 21.23 wt.%, respectively), Fe_2O_3 (avg. 6.72 and 9.40 wt.%, respectively), MgO (avg. 5.21 and 1.10 wt.%, respectively), TiO_2 (avg. 0.88 and 0.23 wt.%, respectively), K_2O (avg. 1.61 and 0.42 wt.%, respectively), and LOI (avg. 6.4 and 14.30 wt.%, respectively). Thus, the claystone samples show increase of Al_2O_3, Fe_2O_3, and LOI, and decrease

https://doi.org/10.1007/s42860-020-00097-3 Published online by Cambridge University Press

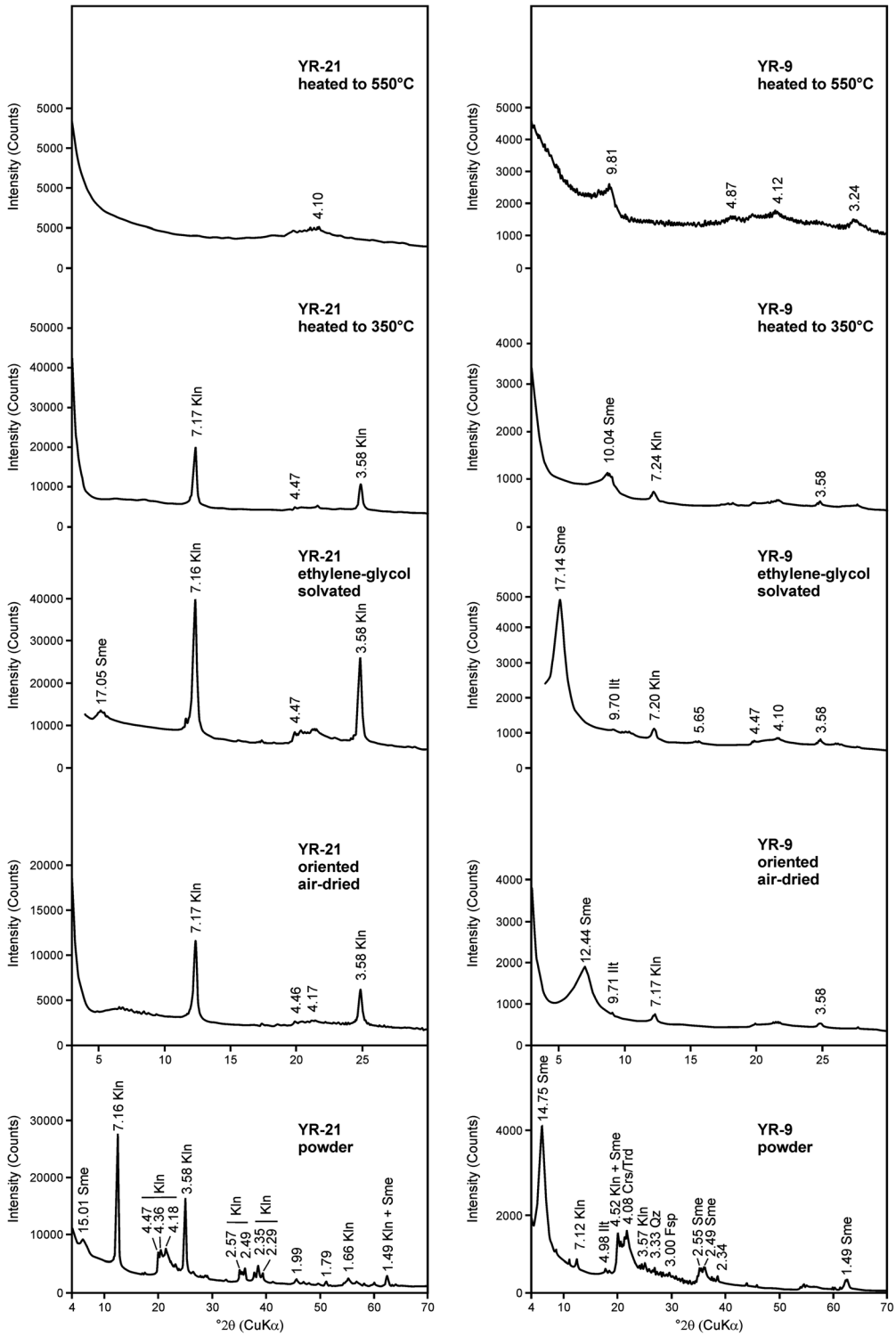

Fig. 6. XRD patterns for clayey material samples from Yarıkçı clay deposit. Sme: smectite; Kln: kaolinite; Ilt/Ms: illite/muscovite; Ilt: illite; Ms: muscovite; Chl: chlorite; Crs/Trd: cristobalite/tridymite; Qz: quartz; Fsp: feldspar; Px: pyroxene (mineral-name abbreviations after Whitney and Evans 2010)

in SiO_2, MgO, and K_2O compared to the parent rocks. The large amounts of Al_2O_3 + LOI and Fe_2O_3 ± TOT/S in claystone units exhibit the presence of kaolinite and smectite. On the other hand, the large Al_2O_3, Fe_2O_3, and K_2O

https://doi.org/10.1007/s42860-020-00097-3 Published online by Cambridge University Press

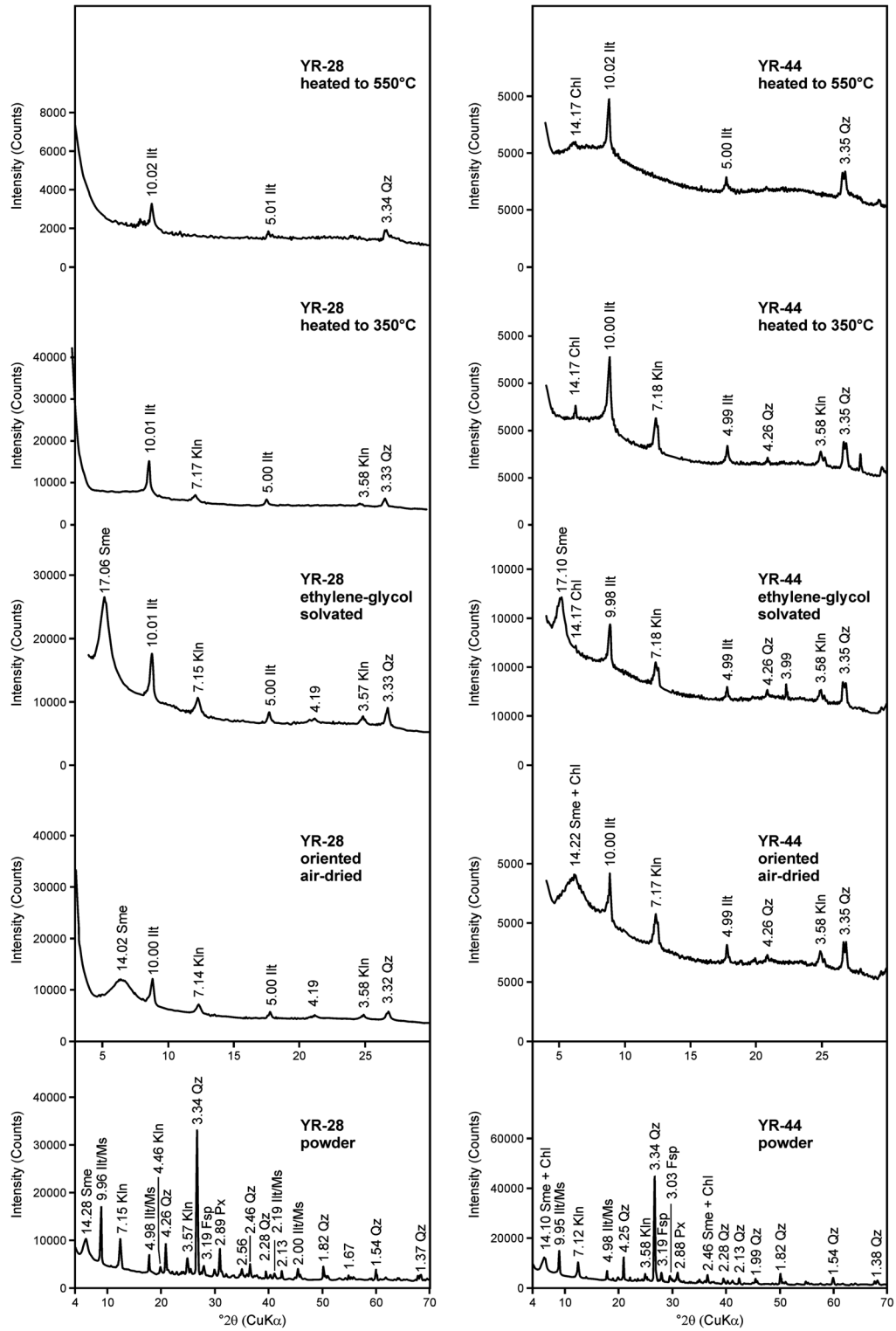

Fig. 6 (continued)

values in the parent schist rocks reflect the presence of muscovite, chlorite, feldspar, and Fe oxides associated with accessory kaolinite and smectite.

The CIW values of the parent rocks, claystones, and silica phases are, on average, 56, 91, and 80, respectively (Table 2). SiO_2 is enhanced up to a maximum of 94.26 wt.%

https://doi.org/10.1007/s42860-020-00097-3 Published online by Cambridge University Press

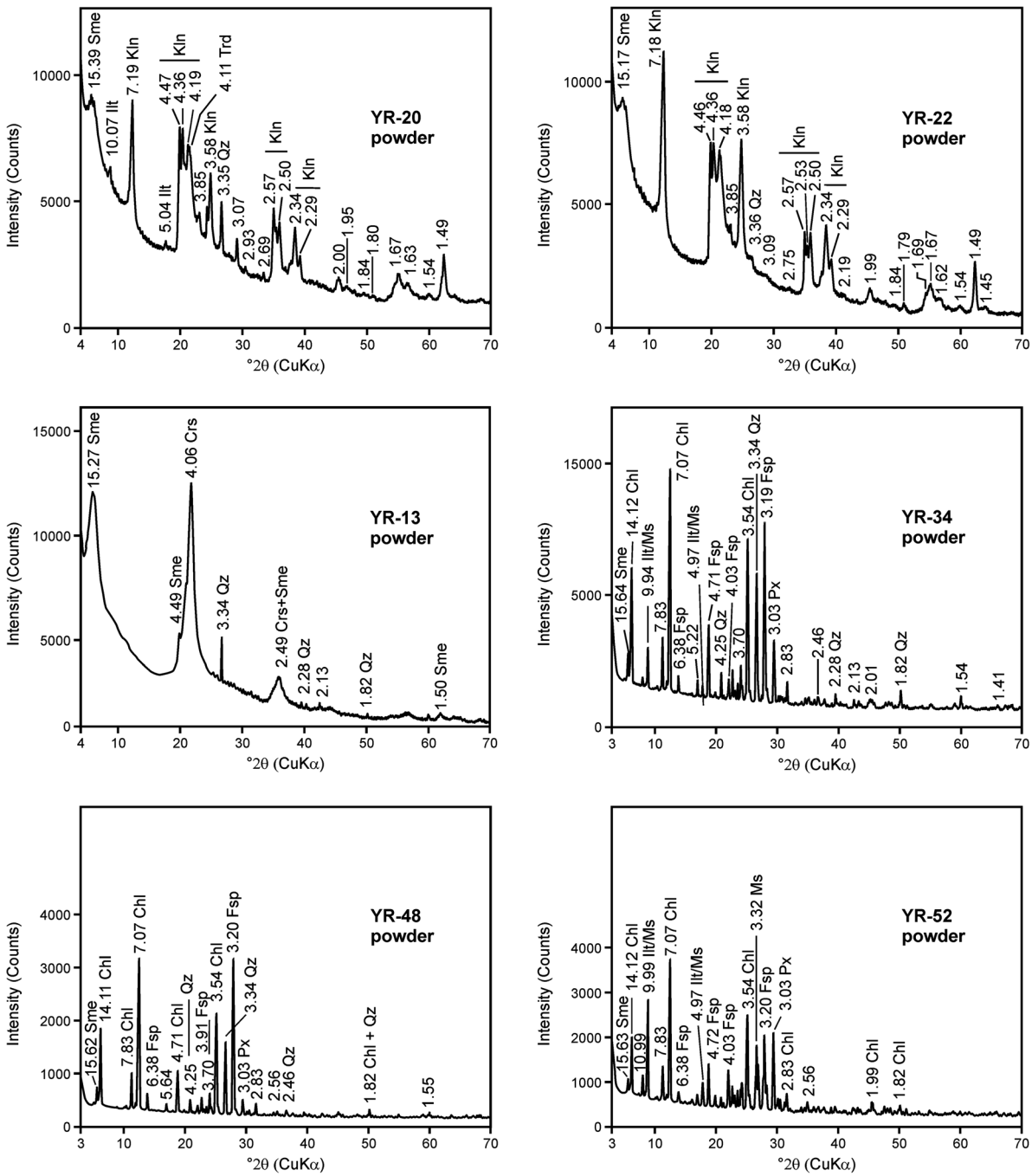

Fig. 6 (continued)

and Au to a maximum of 41.9 ppb in the silica-rich phase, whereas Sr (maximum 231.3 ppm), Cr (maximum 3688 ppm), and Cu (maximum 1087.6 ppm) are significant in claystones. Rb (maximum of 102.6 ppm), Ba (maximum of 294 ppm), Zr (maximum of 145.6 ppm), and Ni (maximum of 102.8 ppm) are at enriched levels in the illitic claystone. In addition, the parent rocks exhibit enhanced amounts of Sr (maximum of 493.6 ppm), Zr (maximum of 163.5 ppm), and Ni (maximum of 86 ppm).

The whole-rock REE contents of both parent-rock samples and related claystone samples were normalized to chondrite (Table 2; Fig. 9). The LREE values display slight enrichment [avg. $(La/Sm)_N$ = 26.5–266.4, avg. $(La/Yb)_N$ = 5.6–12.1, and $(La/Lu)_N$ = 5.6–9.3] relative to MREE+HREE [avg. (Gd/Yb) = 0.8–1.4] and distinct and negative values for both Eu

https://doi.org/10.1007/s42860-020-00097-3 Published online by Cambridge University Press

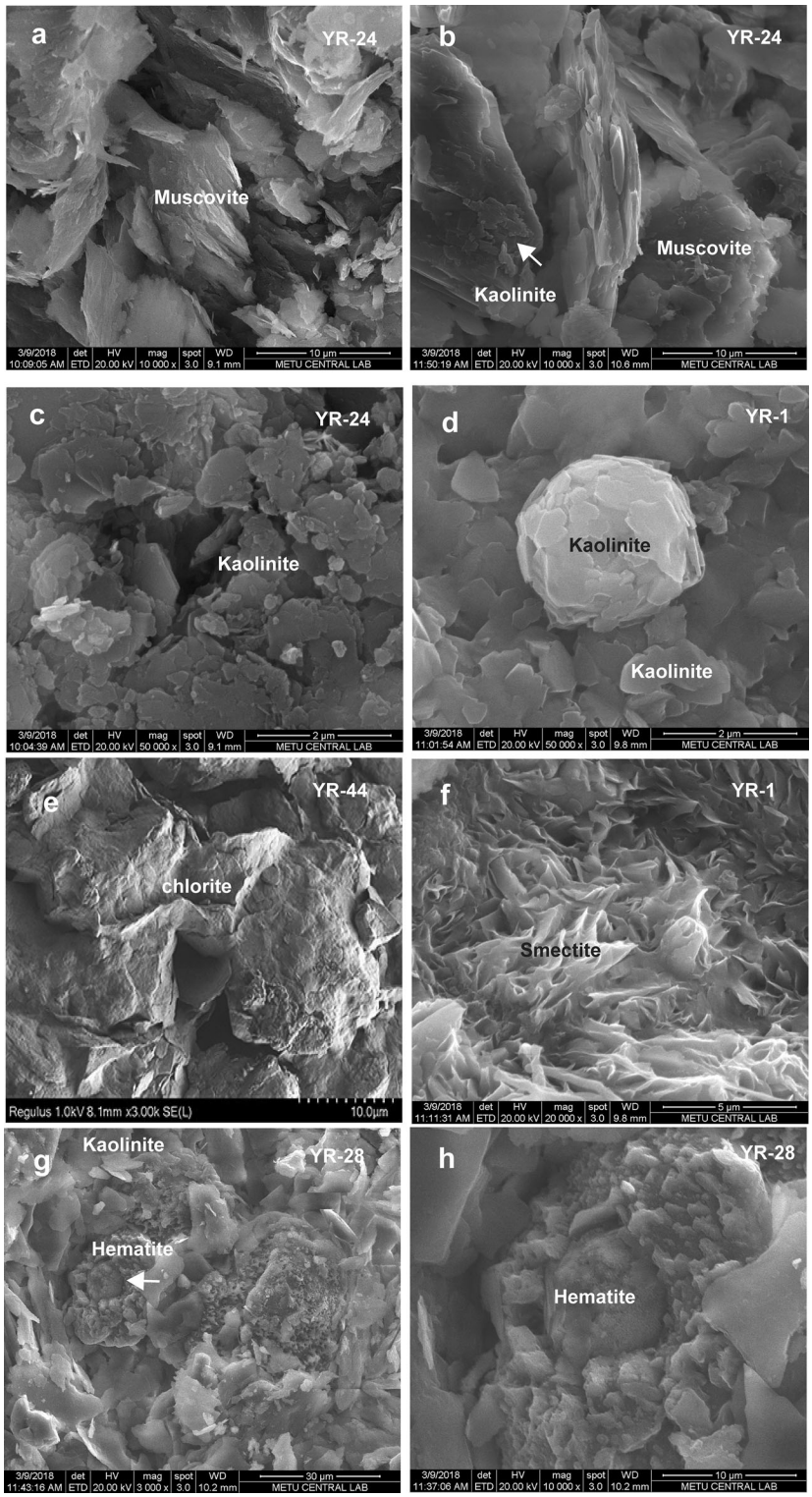

Fig. 7. SEM images of: **a**, **b** muscovite-book flakes edged by platy kaolinite (YR-24); **c** irregular platy kaolinite locally showing hexagonal outlines (YR-24); **d** kaolinite exhibiting sub-rounded book-like structure (YR-1); **e** chlorite platelets (YR-44); **f** flaky smectite (YR-1); **g** sub-rounded disc-shaped hematite and rod-like goethite in pore of kaolinitic materials (YR-28); **h** enlarged view of g; **i** rod- and, locally, star-like goethite formed as a thin film on the surface of opaline (YR-25); **j**, **k** enlarged view of i; **l** subhedral jarosite crystals with altered materials (YR-28); **m**,**n** condensed, irregular, rod-shaped structures making up gypsum/anhydrite (YR-26)

https://doi.org/10.1007/s42860-020-00097-3 Published online by Cambridge University Press

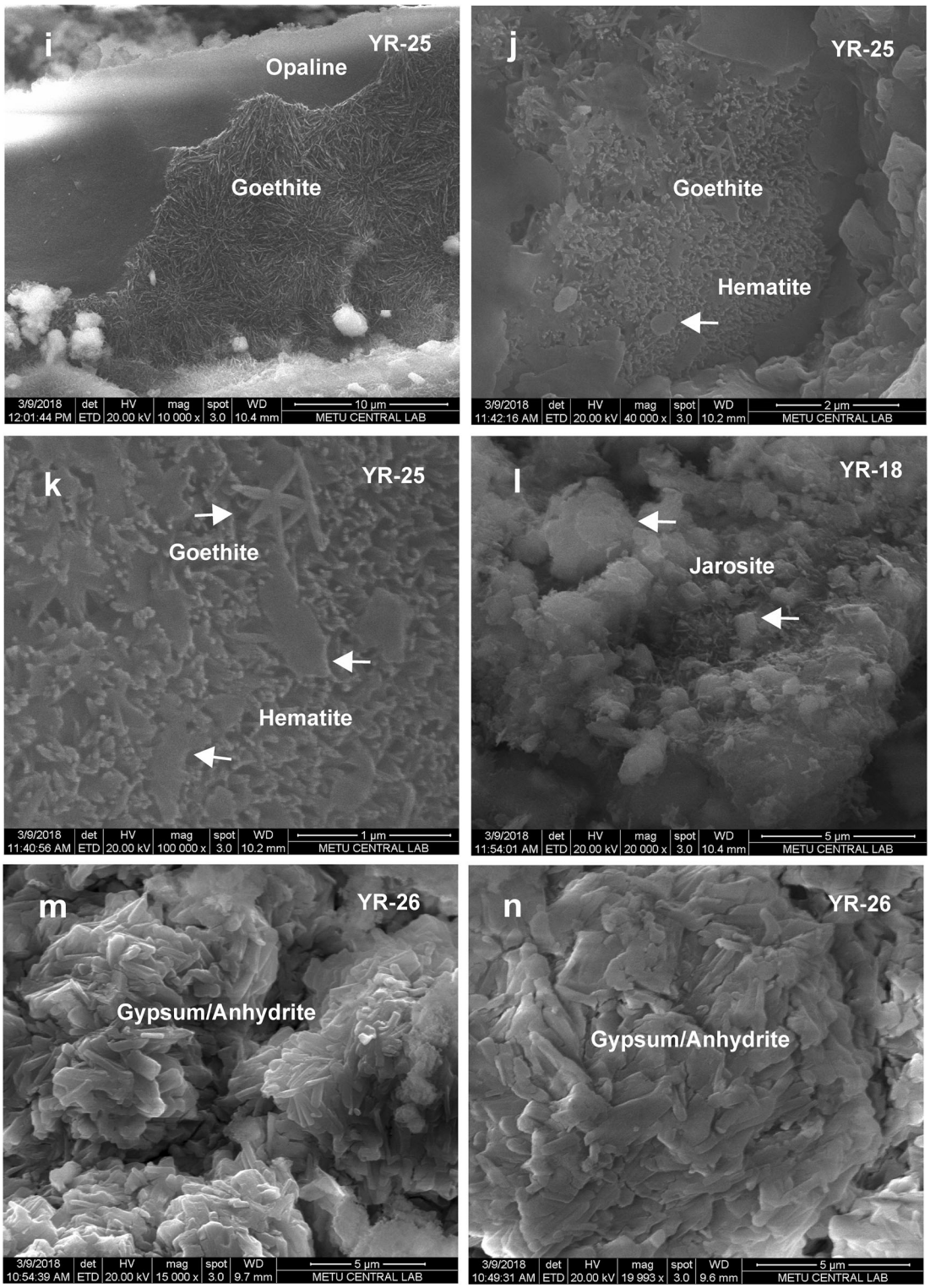

Fig. 7 (continued)

(avg. Eu/Eu* = 0.6–0.3) and Ce (avg. Ce/Ce* = 0.9–0.3) anomalies (Table 2; Fig. 9).

The mass gains and losses were based on calculated delta (ΔC_i) and the plots of the geochemical analyses on isocon

https://doi.org/10.1007/s42860-020-00097-3 Published online by Cambridge University Press

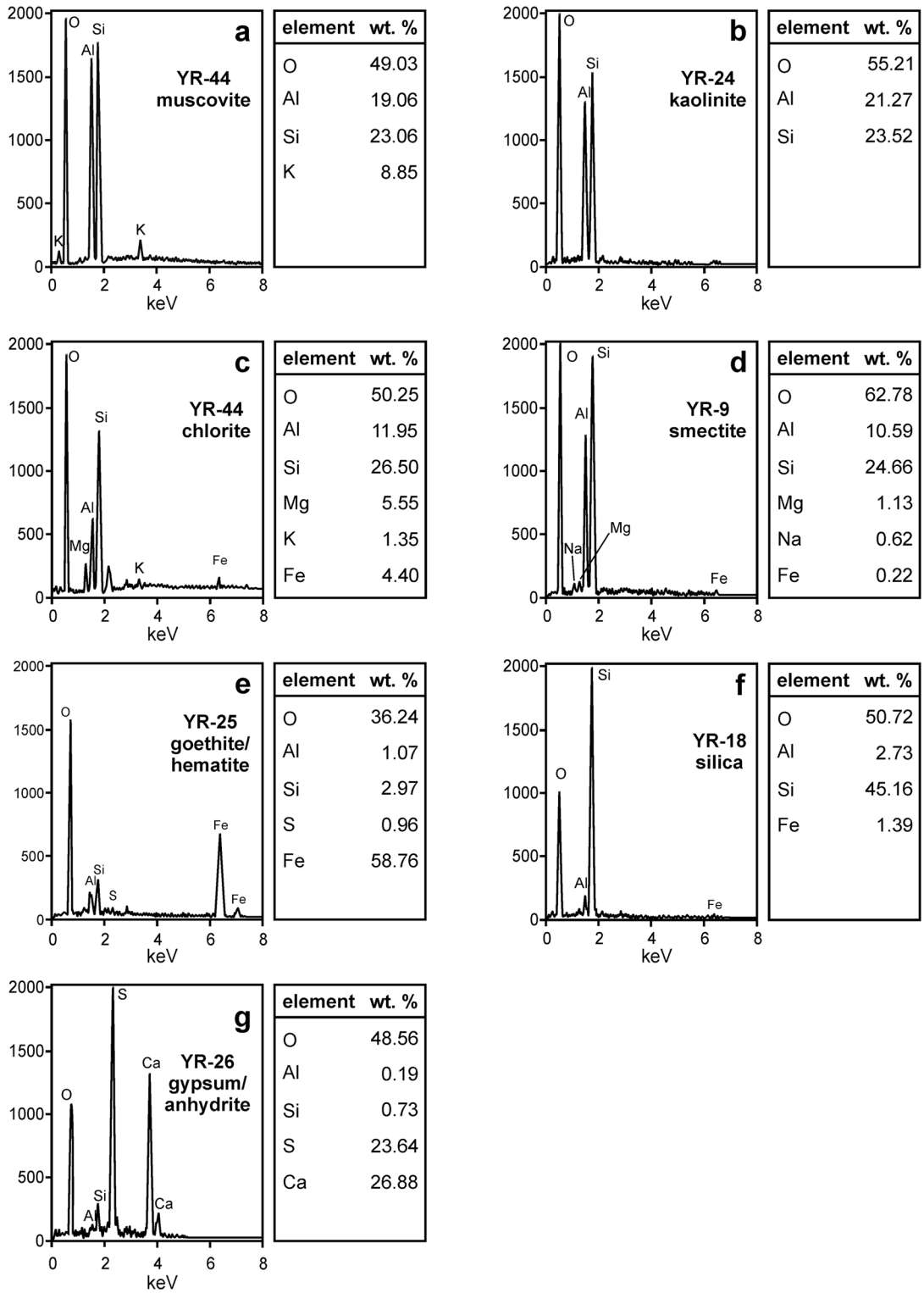

Fig. 8. EDX analyses of: **a** muscovite; **b** kaolinite; **c** chlorite; **d** smectite; **e** goethite/hematite; **f** silica; **g** gypsum/anhydrite

diagrams (Grant 1986, 2005) show that MgO, CaO, Na_2O, K_2O, SiO_2, TiO_2, MnO, Sr, Ba, Rb, Nb, Th, Hf, Y, Ni, and Zr were depleted, while Al_2O_3, Fe_2O_3, As, Cs, V, U, and Cr were enriched during the hydrothermal alteration process based on

https://doi.org/10.1007/s42860-020-00097-3 Published online by Cambridge University Press

Table 2. Major oxide (wt.%), minor element, and trace element (ppm) contents of the parent rocks, claystone, and silica samples in the study area (see Table 1 for the mineralogical compositions of the samples)

Major oxides (wt.%)	Parent rock							Claystone				
	YR-47	YR-48	YR-52	YR-46	YR-50	YR-51	avg.	YR-1	YR-5	YR-9	YR-14	YR-19
SiO_2	49.56	55.07	49.17	54.45	63.04	67.33	56.44	59.93	54.21	67.09	56.61	59.34
Al_2O_3	15.66	15.55	18.23	11.70	17.16	13.88	15.36	19.44	28.81	14.97	23.18	26.12
Fe_2O_3	6.88	8.49	7.03	5.50	6.41	6.04	6.72	2.16	0.55	1.23	1.00	0.65
MgO	6.75	5.08	3.78	8.59	2.99	4.08	5.21	1.25	0.56	1.54	1.39	0.32
CaO	5.99	3.70	7.77	5.10	0.37	0.42	3.89	0.73	0.42	0.26	0.60	0.03
Na_2O	3.69	4.89	3.85	2.22	1.89	0.68	2.87	0.41	1.42	0.22	0.67	0.46
K_2O	0.72	0.03	1.96	1.26	2.96	2.73	1.61	0.23	0.13	0.12	0.37	0.29
TiO_2	1.16	1.24	0.97	0.52	0.77	0.62	0.88	0.33	0.08	0.11	0.08	0.18
P_2O_5	0.14	0.18	0.12	0.13	0.14	0.11	0.14	<0.01	<0.01	<0.01	<0.01	<0.01
MnO	0.21	0.12	0.07	0.10	0.21	0.12	0.14	<0.01	<0.01	<0.01	<0.01	<0.01
Cr_2O_3	0.060	0.003	0.055	0.012	0.023	0.017	0.028	0.344	0.118	0.202	0.336	0.055
TOT/S	<0.02	<0.02	0.02	<0.02	0.02	<0.02	<0.02	0.02	<0.02	<0.02	<0.02	0.18
TOT/C	1.33	0.62	1.08	2.07	0.46	0.36	0.99	0.03	0.02	0.04	0.02	<0.02
LOI	8.9	5.5	6.7	10.2	3.8	3.8	6.4	15.1	13.7	14.2	15.6	12.5
Total	99.80	99.83	99.82	99.79	99.85	99.85	99.82	99.90	99.95	99.93	99.91	99.97
CIW	48.0	51.2	47.0	20.4	81.9	88.3	56.1	90.7	90.3	94.8	91.5	97.1
Trace elements (ppm)												
Ba	92	19	434	221	349	299	235.6	29	15	7	27	6
Be	<1	<1	<1	<1	3	3	1.6	<1	<1	<1	<1	<1
Co	32.9	25.5	18.4	14.4	16.4	23.7	21.9	4.1	2.2	3.0	5.0	4.2
Cr	411	21	376	82	157	116	194	2354	807	1382	2299	376
Cs	1.6	<0.1	3.6	3.3	7.0	6.3	3.65	51.2	33.9	6.6	44.6	7.9
Ga	13.3	15.2	16.8	11.9	18.7	15	15.1	15	16	11.3	10.5	12.2
Hf	2.2	2.9	2.1	3.9	4.2	3.1	3.0	<0.1	<0.1	0.2	0.1	<0.1
Nb	7.8	10.2	10.8	7.5	14.3	10.8	10.2	0.6	<0.1	0.2	<0.1	<0.1
Rb	25.9	0.2	57.8	44.2	112.3	102.8	57.2	12.8	7.0	3.2	13.5	7.4
Sn	2	<1	1	1	2	2	1.5	<1	<1	<1	<1	<1
Sr	150.9	121.6	493.6	64.1	53.1	44	154.5	94.3	231.3	38.3	147.4	26.4
Ta	0.6	0.6	0.7	0.6	0.9	0.8	0.7	<0.1	<0.1	<0.1	<0.1	<0.1
Th	1.2	1.7	1.9	6.2	10.2	5.4	4.4	<0.2	<0.2	<0.2	<0.2	<0.2
U	0.9	0.6	1.2	1.1	1.2	1.4	1.0	0.4	0.5	1.8	0.6	1.5
V	220	229	151	98	154	120	162	311	103	231	258	169
W	2.6	<0.5	1.4	<0.5	0.9	1.9	1.3	<0.5	<0.5	<0.5	<0.5	<0.5
Zr	84.3	103.6	79.2	156.3	163.5	119.5	117.7	2.6	1.2	5.8	6.1	2.3
Y	22.2	21.4	13.9	15	14.4	23.6	18.4	0.2	0.2	0.1	0.8	0.1
La	5.4	10.7	10.0	17.7	30.3	16.7	15.1	0.7	0.8	0.5	0.8	0.8
Ce	11.2	23.7	18.3	35.6	62.7	43.1	32.4	0.2	0.2	0.2	1.2	0.1
Pr	1.61	2.97	2.42	3.98	7.04	3.88	3.65	0.02	0.02	0.04	0.2	<0.02
Nd	7.9	12.7	10.5	14.0	25.4	14.8	14.1	<0.3	<0.3	<0.3	0.9	<0.3
Sm	2.06	3.15	2.43	3.04	4.98	2.94	3.1	<0.05	<0.05	<0.05	0.10	<0.05
Eu	0.71	1.05	1.15	0.77	1.02	0.7	0.9	<0.02	<0.02	<0.02	0.05	<0.02
Gd	3.05	3.95	2.59	3.12	4.31	3.11	3.35	<0.05	<0.05	<0.05	0.19	<0.05
Tb	0.56	0.62	0.43	0.49	0.6	0.56	0.54	<0.01	<0.01	<0.01	0.02	<0.01
Dy	3.74	4.09	2.73	2.95	3.10	3.80	3.4	0.07	<0.05	<0.05	0.18	<0.05
Ho	0.88	0.85	0.56	0.57	0.57	0.91	0.72	<0.02	<0.02	<0.02	0.03	<0.02

https://doi.org/10.1007/s42860-020-00097-3 Published online by Cambridge University Press

Table 2. (continued)

Major oxides (wt.%)	Parent rock							Claystone				
	YR-47	YR-48	YR-52	YR-46	YR-50	YR-51	avg.	YR-1	YR-5	YR-9	YR-14	YR-19
Er	2.37	2.48	1.46	1.62	1.60	2.64	2.02	0.04	<0.03	<0.03	0.07	<0.03
Tm	0.36	0.36	0.22	0.23	0.24	0.38	0.28	<0.01	<0.01	<0.01	<0.01	<0.01
Yb	2.32	2.42	1.34	1.55	1.68	2.38	1.95	<0.05	<0.05	<0.05	0.11	<0.05
Lu	0.35	0.36	0.22	0.24	0.26	0.35	0.30	<0.01	<0.01	<0.01	<0.01	<0.01
Pb	6.3	1.6	6.5	2.2	8.1	4.0	4.8	<0.1	<0.1	<0.1	<0.1	0.2
Zn	36	48	51	38	79	74	54.3	1	<1	2	1	2
Ni	69.3	19.1	66.1	37.1	69.6	86	57.8	9.9	3.7	14.7	21.7	15.2
Au (ppb)	<0.5	<0.5	1.7	1.3	1.0	<0.5	0.9	3.9	<0.5	<0.5	<0.5	<0.5
Ag	<0.1	<0.1	<0.1	<0.1	<0.1	<0.1	<0.1	<0.1	<0.1	<0.1	<0.1	<0.1
Mo	<0.1	0.3	0.2	0.1	0.1	0.3	0.1	<0.1	<0.1	0.3	0.1	0.2
Cu	61.9	23.6	75.0	10.2	2.8	5.5	29.8	90.9	25.9	54.8	40.3	48.2
As	2.3	4.2	1.2	<0.5	2.5	1.5	2.0	3.5	<0.5	9.0	4.5	3.3
Cd	<0.1	<0.1	<0.1	<0.1	<0.1	<0.1	<0.1	<0.1	<0.1	<0.1	<0.1	<0.1
Sb	<0.1	<0.1	<0.1	<0.1	<0.1	<0.1	<0.1	<0.1	<0.1	<0.1	<0.1	<0.1
Bi	<0.1	<0.1	<0.1	<0.1	0.2	0.3	0.1	<0.1	<0.1	<0.1	<0.1	<0.1
Hg	0.03	0.03	0.07	<0.01	<0.01	<0.01	0.03	<0.01	<0.01	<0.01	<0.01	<0.01
Tl	<0.1	<0.1	<0.1	<0.1	<0.1	<0.1	<0.1	<0.1	<0.1	<0.1	<0.1	<0.1
Se	<0.5	<0.5	<0.5	<0.5	<0.5	<0.5	<0.5	<0.5	<0.5	<0.5	<0.5	<0.5
∑REE	64.71	90.8	68.25	84.24	143.8	96.2	91.3	1.75	1.82	1.44	4.67	1.62
∑LREE	26.11	50.07	41.22	71.28	125.44	78.48	65.4	1.22	1.32	1.04	3.1	1.22
∑MREE	11	13.71	9.89	10.94	14.58	12.02	12.02	0.22	0.2	0.2	0.57	0.2
∑HREE	5.4	5.62	3.24	3.64	3.78	5.75	4.6	0.11	0.1	0.1	0.2	0.1
Eu/Eu*	0.9	0.9	0.4	0.7	0.6	0.1	0.6	0.3	0.3	0.3	0.3	0.3
Ce/Ce*	0.9	1.0	0.8	0.9	0.9	1.2	0.9	0.1	0.1	0.2	0.7	0.06
$(La/Sm)_N$	1.6	2.1	62.2	3.6	3.8	85.9	26.5	211.7	241.9	151.2	120.9	241.9
$(La/Yb)_N$	1.5	2.9	5.0	7.7	12.1	4.7	5.6	9.4	10.8	6.7	4.9	10.8
$(La/Lu)_N$	1.6	3.0	4.7	7.6	12.0	4.9	5.6	7.2	8.3	5.1	8.3	8.3
$(Gd/Yb)_N$	1.0	1.3	1.5	1.6	2.0	1.0	1.4	0.8	0.8	0.8	1.3	0.8

Major oxides (wt.%)	Claystone					Silica phase							
	YR-23	YR-7	YR-24	YR-28	avg.	YR-2a	YR-4a	YR-15	YR-8a	YR-16	YR-17	YR-26a	avg.
SiO_2	48.37	29.92	40.38	49.55	51.71	85.53	80.31	76.78	70.93	82.25	76.77	94.26	80.98
Al_2O_3	32.98	2.62	27.45	15.49	21.23	3.99	5.88	7.31	16.46	4.95	6.16	0.65	6.49
Fe_2O_3	2.48	52.37	15.82	8.38	9.40	1.26	1.17	1.50	0.47	1.20	2.26	0.44	1.19
MgO	0.32	0.33	0.18	3.97	1.10	0.84	1.18	1.04	0.40	0.88	1.51	0.22	0.87
CaO	0.03	0.04	0.02	4.89	0.78	0.34	0.55	0.32	0.18	0.11	0.13	0.10	0.25
Na_2O	<0.01	0.08	<0.01	0.62	0.43	0.09	0.07	0.10	1.34	0.03	0.02	0.06	0.24
K_2O	0.02	0.02	0.01	2.56	0.42	0.04	0.03	0.12	0.38	0.08	0.04	0.02	0.10
TiO_2	0.27	0.04	0.27	0.73	0.23	0.18	0.31	0.28	0.13	0.18	0.27	0.16	0.22
P_2O_5	<0.01	<0.01	<0.01	0.10	0.02	<0.01	<0.01	0.01	0.01	<0.01	0.03	<0.01	0.01
MnO	<0.01	<0.01	<0.01	0.17	0.03	<0.01	<0.01	<0.01	<0.01	<0.01	<0.01	<0.01	0.01
Cr_2O_3	0.260	0.273	0.539	0.021	0.24	0.758	0.722	1.113	0.071	0.822	0.932	0.133	0.65
TOT/S	0.09	0.50	0.21	<0.02	0.12	0.04	<0.02	<0.02	<0.02	<0.02	<0.02	0.11	0.04
TOT/C	0.02	0.03	<0.02	2.13	0.26	<0.02	<0.02	0.03	<0.02	<0.02	0.03	0.02	0.02
LOI	15.2	13.9	15.2	13.3	14.30	6.9	9.6	11.3	9.6	9.4	11.7	3.9	8.91
Total	99.93	99.62	99.91	99.83	99.88	99.93	99.91	99.88	99.96	99.89	99.88	100.01	99.92

https://doi.org/10.1007/s42860-020-00097-3 Published online by Cambridge University Press

Table 2. (continued)

Major oxides (wt.%)	Parent rock							Claystone					
	YR-47	YR-48	YR-52	YR-46	YR-50	YR-51	avg.	YR-1	YR-5	YR-9	YR-14	YR-19	
CIW	99.8	94.4	99.8	60.9	91.0	84.7	84.1	91.0	86.7	97.0	20.5	96.9	80.1
Trace elements (ppm)													
Ba	5	2	3	294	43.11	23	12	24	18	19	9	3	15.43
Be	<1	<1	<1	<1	1.00	<1	<1	<1	<1	<1	<1	<1	1.00
Co	7.7	2.2	6.7	31.9	7.44	12	2.8	5.4	1.6	9.0	18.8	14.4	9.14
Cr	1779	1868	3688	144	1633	5186	4940	7615	486	5624	6377	910	4448
Cs	1.4	6.9	1.4	11.8	18.41	20.7	18	60.9	18.1	55.6	28.8	10.2	30.33
Ga	18.8	6.4	21.3	17.0	14.28	5.3	6.5	6.1	9.6	5.1	5.6	<0.5	5.53
Hf	0.2	0.1	0.1	4.2	0.58	0.1	0.2	0.2	0.2	0.1	0.1	0.3	0.17
Nb	<0.1	0.1	<0.1	12.6	1.56	0.6	0.6	0.4	0.3	0.1	<0.1	0.1	0.31
Rb	0.2	1.0	0.2	102.6	16.43	4.4	3.1	1.44	10.3	7.2	3.4	1.1	4.42
Sn	<1	<1	<1	3	1.22	<1	<1	<1	<1	<1	<1	<1	1.00
Sr	2.6	4.8	1.1	179.6	80.64	35.9	30.4	31.6	198.7	21.5	15.7	10.8	49.23
Ta	<0.1	<0.1	<0.1	0.8	0.18	<0.1	<0.1	<0.1	<0.1	<0.1	<0.1	<0.1	0.10
Th	<0.2	<0.2	0.4	10.7	1.39	<0.2	<0.2	<0.2	<0.2	<0.2	<0.2	<0.2	0.20
U	2.0	0.7	2.1	2.3	1.32	<0.1	1.0	0.4	3.9	1.1	2.4	1.1	1.43
V	331	1237	322	148	345.6	336	445	534	77	459	429	27	329.6
W	<0.5	<0.5	<0.5	4.3	0.92	<0.5	<0.5	<0.5	<0.5	<0.5	<0.5	0.5	0.50
Zr	3.8	3.6	4.2	145.6	19.47	2	3.2	5.4	6.5	4.0	3.7	4.8	4.23
Y	0.1	<0.1	0.2	24.9	2.97	0.1	0.1	0.3	0.3	0.2	0.1	0.4	0.21
La	0.4	0.4	0.5	30.9	3.98	1.4	0.9	1.1	0.9	0.5	0.7	0.8	0.90
Ce	0.4	0.2	<0.1	68.2	7.87	0.4	0.4	0.3	0.3	0.3	0.4	0.5	0.37
Pr	0.03	<0.02	<0.02	26.7	3.01	<0.02	0.02	0.02	<0.02	0.03	0.03	0.09	0.03
Nd	<0.3	<0.3	<0.3	26.7	3.30	<0.3	<0.3	<0.3	<0.3	<0.3	<0.3	0.3	0.30
Sm	<0.05	<0.05	<0.05	4.99	0.60	<0.05	<0.05	<0.05	<0.05	<0.05	<0.05	0.06	0.05
Eu	<0.02	<0.02	<0.02	1.11	0.14	<0.02	<0.02	<0.02	<0.02	<0.02	<0.02	<0.02	0.02
Gd	<0.05	<0.05	<0.05	4.55	0.57	<0.05	<0.05	<0.05	<0.05	<0.05	<0.05	0.08	0.05
Tb	<0.01	<0.01	<0.01	0.74	0.09	<0.01	<0.01	<0.01	<0.01	<0.01	<0.01	<0.01	0.01
Dy	<0.05	<0.05	0.06	4.42	0.55	<0.05	<0.05	<0.05	0.08	<0.05	<0.05	0.09	0.06
Ho	<0.02	<0.02	<0.02	0.96	0.13	<0.02	<0.02	<0.02	<0.02	<0.02	<0.02	<0.02	0.02
Er	<0.03	<0.03	<0.03	2.71	0.33	<0.03	<0.03	<0.03	0.04	<0.03	<0.03	<0.03	0.03
Tm	<0.01	<0.01	<0.01	0.40	0.05	<0.01	<0.01	<0.01	<0.01	<0.01	<0.01	<0.01	0.01
Yb	<0.05	<0.05	<0.05	2.64	0.34	<0.05	<0.05	<0.05	0.05	<0.05	<0.05	<0.05	0.05
Lu	<0.01	<0.01	<0.01	0.40	0.05	<0.01	<0.01	<0.01	<0.01	<0.01	<0.01	<0.01	0.01
Pb	<0.1	0.4	0.2	19.6	2.32	<0.1	<0.1	<0.1	<0.1	<0.1	0.1	0.2	0.11
Zn	2	2	6	118	15.00	<1	<1	<1	<1	2	6	2	2.00
Ni	29.4	7.0	23.6	102.8	25.33	22.5	13.1	8.1	3.9	21.0	91.8	44.6	29.29
Au (ppb)	4.2	8.6	5.0	<0.5	2.69	0.5	<0.5	2.4	0.9	1.4	41.9	<0.5	6.87
Ag	<0.1	<0.1	<0.1	<0.1	0.10	<0.1	<0.1	<0.1	<0.1	<0.1	<0.1	<0.1	0.10
Mo	0.5	0.5	1.8	1.2	0.53	<0.1	<0.1	<0.1	<0.1	0.5	<0.1	0.1	0.16
Cu	29.4	1087.6	281.6	38.7	188.6	12.9	8.9	35.9	32.1	79.2	164.3	11.1	49.20
As	8.1	64.8	13.8	27.0	14.94	1.9	0.7	14.9	2.1	15.2	4.8	1.3	5.84
Cd	<0.1	<0.1	<0.1	<0.1	0.10	<0.1	<0.1	<0.1	<0.1	<0.1	<0.1	<0.1	0.10
Sb	<0.1	<0.1	<0.1	<0.1	0.10	<0.1	<0.1	<0.1	<0.1	<0.1	<0.1	<0.1	0.10
Bi	<0.1	<0.1	<0.1	0.3	0.12	<0.1	<0.1	<0.1	<0.1	<0.1	<0.1	<0.1	0.10
Hg	<0.01	<0.01	<0.01	<0.01	0.01	<0.01	<0.01	<0.01	<0.01	<0.01	<0.01	<0.01	0.01

https://doi.org/10.1007/s42860-020-00097-3 Published online by Cambridge University Press

Table 2. (continued)

Major oxides (wt.%)	Parent rock							Claystone					
	YR-47	YR-48	YR-52	YR-46	YR-50	YR-51	avg.	YR-1	YR-5	YR-9	YR-14	YR-19	
Tl	<0.1	<0.1	<0.1	<0.1	0.10	<0.1	<0.1	<0.1	<0.1	<0.1	<0.1	<0.1	0.10
Se	<0.5	1.4	<0.5	<0.5	0.60	<0.5	<0.5	<0.5	<0.5	<0.5	<0.5	<0.5	0.50
∑REE	1.53	1.32	1.43	200.3	23.99	2.52	2.02	2.32	2.16	1.63	1.83	2.47	2.14
∑LREE	1.13	0.92	0.92	152.5	18.15	2.12	1.62	1.72	1.52	1.13	1.43	1.69	1.60
∑MREE	0.2	0.2	0.21	16.77	2.09	0.2	0.2	0.2	0.23	0.2	0.2	0.28	0.22
∑HREE	0.1	0.1	0.1	6.15	43.11	0.1	0.1	0.1	0.11	0.1	0.1	0.1	15.43
Eu/Eu*	0.3	0.3	0.3	0.2	0.3	0.3	0.3	0.3	0.3	0.3	0.3	0.3	0.3
Ce/Ce*	0.4	0.2	0.1	1.0	0.3	0.1	0.2	0.1	0.1	0.3	0.3	0.3	0.2
$(La/Sm)_N$	120.9	120.9	151.2	93.6	161.5	423.4	272.2	332.6	272.2	151.2	211.7	201.6	266.4
$(La/Yb)_N$	5.4	5.4	6.7	7.9	7.5	18.9	12.1	14.8	12.1	6.7	9.4	10.8	12.1
$(La/Lu)_N$	4.1	4.1	5.1	8.0	6.5	14.5	9.3	11.4	9.3	5.1	7.2	8.3	9.3
$(Gd/Yb)_N$	0.8	0.8	0.8	1.3	0.9	0.8	0.8	0.8	0.8	0.8	0.8	1.2	0.8

REE = the sum of (La–Lu)+Y; LREE = the sum of La–Nd; MREE = the sum of (Sm–Ho); HREE = the sum of (Er–Lu); Eu/Eu* = $Eu_N/[(Sm_N x0.67)+(Tb_N x0.33)]$ (Bau and Dulski 1996) and Ce/Ce* = $3Ce_N/(2La_N+Nd_N)$ (Mongelli 1997). N refers to a chondrite-normalized value (Taylor and McLennan 1985). LOI: loss on ignition at 1050°C

isocon slope (m = 1) (Table 3; Fig. 10a–c). Tl shows immobile character. Zr/Ni shows positive correlation with Zr/Co (r^2 = 0.5492) (Fig. 11).

DISCUSSION

Alteration developed as a result of NW–SE- and N–S-trending, structurally controlled hydrothermal activity in the Mesozoic chlorite schist, muscovite schist, chlorite-muscovite schist, and basement units comprising garnet-graphite, phyllite-type, greenschist facies (Fig. 12). The vertical mineralogical zonation in the clay deposit from bottom to top are characterized by illite, kaolinite, kaolinite-bearing smectite, smectite, and silica cap (Figs. 3, 4, and 12). The increase in CIW values in the claystone (avg. 91) and silica phase (avg. 80) samples compared to the schist-type parent rock samples indicate the occurrence of intense alteration processes. Development of the Fe oxide and silica-phase vein infills, stockwork

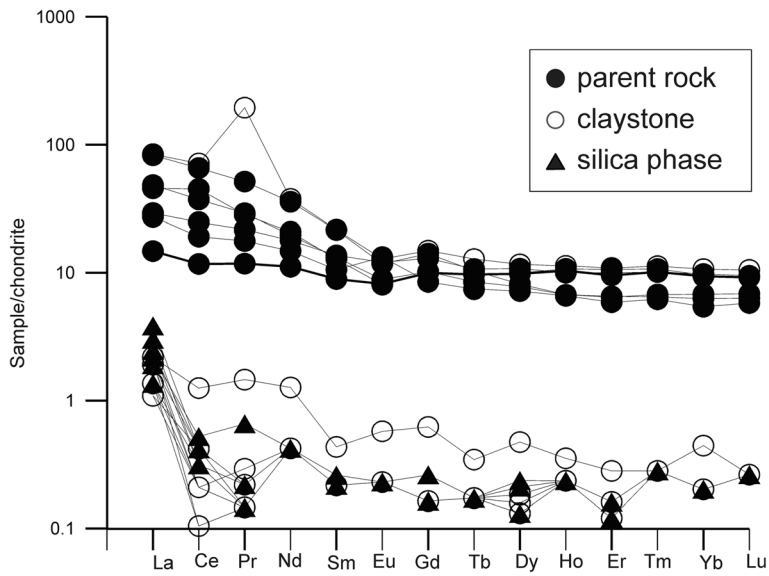

Fig. 9. Chondrite-normalized (Taylor and McLennan 1985) REE spider diagrams for the metamorphic and related altered materials from the Yarıkçı deposit

https://doi.org/10.1007/s42860-020-00097-3 Published online by Cambridge University Press

Table 3. Mass gains and losses of major oxides (g) and trace elements (ppm) for the claystone based on the isocon analysis diagram (Grant 1986, 2005; López-Moro 2012)

			Overall volume change (%)	2.30
			Overall mass change (%)	0.00
			Slope	1.00
Sample	Parent rock avg. (n = 6)	Claystone avg. (n = 9)		
Major oxides (wt. %)	Unaltered C_i^0	Altered C^A	Gain/Loss relative to C_i^0 $\Delta C_i/C_i^0$	Gain/Loss in wt.% ΔC_i
SiO_2	56.44	51.71	–0.08	–4.73
TiO_2	0.88	0.23	–0.74	–0.65
Al_2O_3	15.36	21.23	0.38	5.87
Fe_2O_3	6.72	9.40	0.40	2.68
MnO	0.14	0.03	–0.79	–0.11
MgO	5.21	1.10	–0.79	–4.11
CaO	3.89	0.78	–0.80	–3.11
Na_2O	2.87	0.43	–0.85	–2.44
K_2O	1.61	0.42	–0.74	–1.19
P_2O_5	0.14	0.02	–0.86	–0.12
Trace elements (ppm)			Gain/Loss (ppm)	
As	2.00	14.94	6.47	12.94
Cs	3.65	18.41	4.04	14.76
Rb	57.20	16.43	–0.71	–40.77
Ba	235.60	43.11	–0.82	–192.49
Sr	154.50	80.64	–0.48	–73.86
Pb	4.80	2.32	–0.52	–2.48
Cr	193.60	1642.10	7.57	1448.50
Ni	57.80	25.33	–0.56	–32.47
V	162.00	345.60	1.13	183.60
Ga	15.10	14.28	–0.05	–0.82
Zn	54.30	15.00	–0.72	–39.30
Bi	0.10	0.12	0.20	0.02
U	1.00	1.32	0.32	0.32
Zr	117.70	19.47	–0.83	–98.23
Hf	3.00	0.58	–0.81	–2.42
Y	18.40	2.97	–0.84	–15.43
Nb	10.20	1.56	–0.85	–8.64
Ta	0.70	0.18	–0.74	–0.52
Th	4.40	1.39	–0.68	–3.01
Tl	0.10	0.10	0.00	0.00
La	15.10	3.98	–0.74	–11.12
Ce	32.40	7.87	–0.76	–24.53
Pr	3.65	3.01	–0.18	–0.64
Nd	14.10	3.30	–0.77	–10.80
Sm	3.10	0.60	–0.81	–2.50
Eu	0.90	0.14	–0.84	–0.76
Gd	3.35	0.57	–0.83	–2.78
Tb	0.54	0.09	–0.83	–0.45
Dy	3.40	0.55	–0.84	–2.85
Ho	0.72	0.13	–0.82	–0.59
Er	2.02	0.33	–0.84	–1.69
Tm	0.28	0.05	–0.82	–0.23
Yb	1.95	0.34	–0.83	–1.61
Lu	0.30	0.05	–0.83	–0.25

n: number of samples

https://doi.org/10.1007/s42860-020-00097-3 Published online by Cambridge University Press

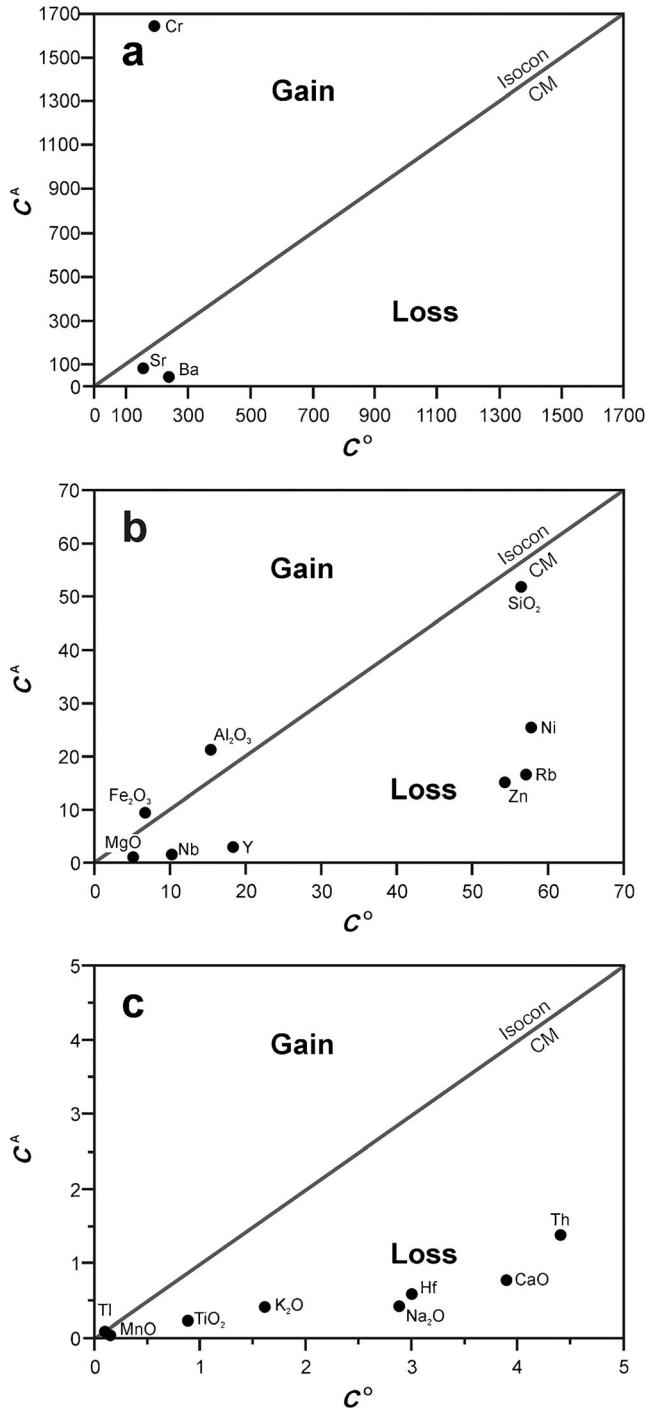

Fig. 10. Mass changes **a**–**c** in the major element (g) and trace element (ppm) contents within the study area based on the isocon analysis diagram (Grant 1986, 2005; López-Moro 2012)

and networks within the clay deposit hosted by schists reveal that smectitization, kaolinization, and silicification occurred under the control of hydrothermal fluid activities (Fig. 12; Nagasawa 1978; Meunier 1995, 2005; Boulais et al. 2000). The occurrence of abundant Fe oxides and cristobalite/tridymite/quartz vein infills, stockworks, and heterogeneous, widely found, cream-, green-, brownish-red-, and gray-colored claystones are related to the presence of goethite/hematite as well as kaolinite, kaolinite-bearing smectite, smectite, and illite contents which also support the assumption of hydrothermal alteration processes related to the Yarıkçı fault zone (Fig. 12; Velde 1985; Meunier 2005). This process was also shown by

https://doi.org/10.1007/s42860-020-00097-3 Published online by Cambridge University Press

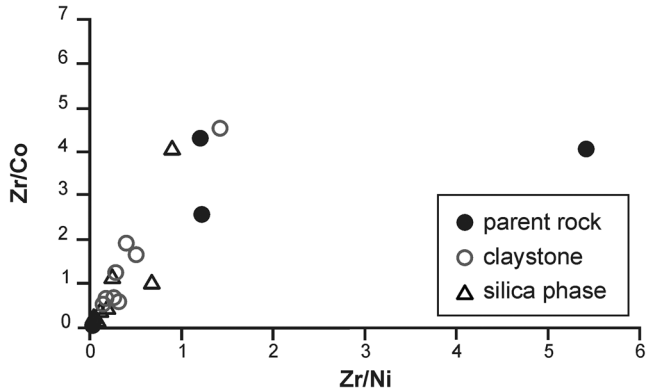

Fig. 11. Elemental variation diagram for Zr/Ni vs. Zr/Co of the Yarıkçı clay deposit samples

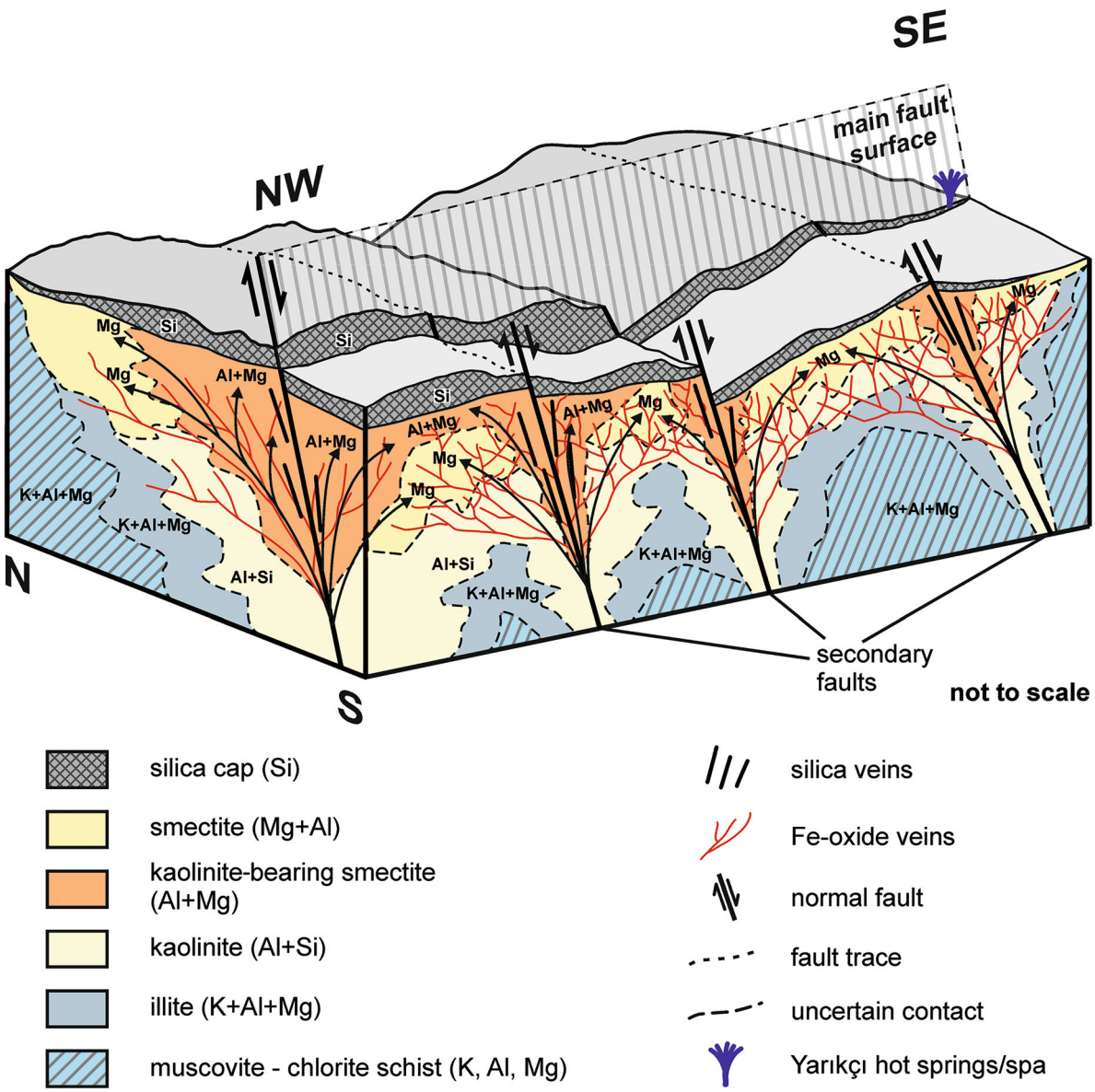

Fig. 12. Sketch of genetic model for the Yarıkçı clay deposit

https://doi.org/10.1007/s42860-020-00097-3 Published online by Cambridge University Press

the contemporary occurrence of the sulfur-bearing Yarıkçı hot springs and spa (temperature of 39°C) situated ~5 km SE of the deposit (Fig. 12). Ömeroğlu Sayıt et al. (2018) also reported that the kaolinite deposit in granitic units of the Ahırözü (Mihalıççık) formed under temperature ranges from 157 to 341°C based on analysis of fluid inclusions in quartz crystals.

Texturally, the development of cataclastic texture such as bending, disaggregation of the quartz crystals, sericitization and argillization of the feldspars, and partial alteration of muscovite and chlorite in muscovite schists, as well as the presence of Fe-(oxyhydr)oxides along the foliation of the schists also reveal the influence of tectonic activities and related alteration of the parent rocks (Fig. 5; Aliyari et al. 2014; Sayın 2016; Taillefer et al. 2017). The lack of Paleocene–Oligocene sedimentary deposits in the study area may suggest that the region was subjected to uplift and fluctuation of the wet-to-dry climatic conditions of the mid- to late-Pleistocene possibly causing the occurrence of chemical weathering similar to that reported by Yılmaz et al. (2000), Külah et al. (2014), and Kadir et al. (2015). However, in this context, progressive tectonism was also responsible for initiating the fault-related hydrothermal alteration process since the Miocene (Şengör et al. 1985). The development of (1) hematite/goethite on kaolinite plates and as films on siliceous material determined by XRD and SEM-EDX analysis and (2) yellow- and brown-colored goethite-bearing claystones and hematite filling subvertical fractures/veins in the upper part of the clay deposit may suggest the influence of Fe during/following the alteration and silicification under both hydrothermal and pedogenic processes. Chen et al. (2018) also reported that the concentration of goethite in the upper part and increased concentration of hematite with depth in the soil profile was indicative of a pedogenic process. Eren and Kadir (2013) and Eren et al. (2015) also stated that the different red coloration in claystone, sandstone, and soil reflect the fluctuation of reducing and oxidizing conditions in the depositional environment. Craw et al. (2009) and Taillefer et al. (2017) also emphasized that flushing of the hydrothermal fluid flow benefits fracturing along the foliation and consequently favored deformation and decreases of the grain sizes of the unit under control of the tectonic stress. The association of chlorite with smectite in chlorite schist may indicate the transformation of chlorite to smectite along the faults similar to those reported for the metamorphic units in the Black Mountains, California (Haines and van der Pluijm 2012). Micromorphologically, the linkage of muscovite with book-like kaolinite may suggest that the alteration of muscovite probably caused the in situ precipitation of kaolinite as a result of dissolution-precipitation under acidic conditions (Exley 1976; Keller 1976).

The depletion of MgO, CaO, Na_2O, K_2O, SiO_2, TiO_2, MnO, Sr, Ba, Rb, Nb, Th, Hf, Y, Ni, and Zr and the enrichment of Al_2O_3, Fe_2O_3, As, Cs, V, U, and Cr during the hydrothermal alteration process of muscovite, chlorite, feldspar, and pyroxenes of the schists have probably caused the downward deposition of the moderately mobile to immobile Al±Fe favoring the precipitation of kaolinite under open acidic environmental conditions (Fig. 12; Parry et al. 1984; Gürsu et al. 2004). In contrast, the increase of Al, Fe, Mg, and alkalis in the upward sequence along the faults favored the formation of smectite under a confined basic hydraulic system (Fig. 12). This can also be explained by the volume of the fluid fluxes. In this context, large fluid fluxes kept the system acidic (pH < 4) and in turn removed reaction products. In contrast, slow fluxes favor reaction products to build and consume acidity and H^+ ions (high pH) in an upward sequence and outwards of the deposit (Inoue 1995; Santamarina et al. 2002; Yalçın and Bozkaya 2003).

The injection of hydrothermal fluids resulted in acidic (pH 3–3.5) conditions and in turn the formation of Fe (oxyhydr)oxides such as goethite and hematite (Schwertmann 1993; Kämpf et al. 2000) filling fractures/veins. The Fe originated from decomposition of pyroxene in the schist rocks. This process was also associated with a silica phase along the tectonically controlled shear zone (MacLean and Barrett 1993; Barrett and MacLean 1994, 1999; Gifkins et al. 2005).

Hydrolysis and the resulting release of excess Si during the alteration processes probably caused the formation of cristobalite/tridymite and quartz (Erhenberg 1991; Meunier and Velde 2004). The development of silicification such as cristobalite/tridymite/quartz veins/stockworks and silica cap and the local enhancement of SiO_2 (maximum 94.26 wt.%), Fe_2O_3 (maximum 52.37 wt.%), TOT/S (maximum 0.5 wt.%), Cu (maximum 1087.6 ppm), and Au (maximum 41.9 ppb) also supported the assumption of the occurrence of a hydrothermal process (Kadir and Akbulut 2009; Acarlioğlu et al. 2013).

The large amounts of Sr (maximum 493.6 ppm), Rb (maximum 102.6 ppm), Ba (maximum 294 ppm), and Zr (maximum 145.6 ppm) were attributed to a metamorphic origin, whereas Cr (maximum 7615 ppm), Ni (maximum 102.8 ppm), and V (maximum 1237 ppm) exhibit ophiolitic contributions and low elemental mobility during the alteration process (Dill et al. 1997; Vidal 1998). High values of Cr in both claystones and silica phase relative to fresh metamorphic units indicate that the ophiolitic units which cropped out in the north may have contributed to the alteration of chlorite to kaolinite in the metamorphic basement units. The mass losses of Sr (in relation to Ca), Rb, and Ba (in relation to K) were due to the alteration of K-bearing minerals such as K-feldspar and muscovite in schist units similar to what was reported for quartz-sericite schists in the Nondweni Greenstone belt (South Africa) by Jele (2013). The positive correlation between Zr/Co and Zr/Ni reflect the fractionation of muscovite, garnet, plagioclase, and K-feldspars rather than pyroxene in the schists (Fraser et al. 1997; Degeling et al. 2001; Bea et al. 2006; Aydınçakır and Şen 2013; Ghanem and Jarrar 2013; Wang et al. 2015).

The slight enrichment in LREE relative to MREE+HREE and negative Eu anomaly may suggest the fractionation of feldspar under the influence of the hydrothermal alteration (McFarlane et al. 2007; Lee et al. 2009; Aliyari et al. 2014; Sayın 2016; Maulana et al. 2019).

The negative Eu anomaly indicates that although Eu^{2+} is stable in the high hydrothermal fluid system, it is more

https://doi.org/10.1007/s42860-020-00097-3 Published online by Cambridge University Press

mobile and rapidly oxidized to Eu^{3+} in the greenschist facies under possibly low hydrothermal temperatures and oxidizing conditions (Sverjensky 1982; Spry et al. 2007; Serna 2014). The negative Ce anomaly may be related to the leaching of Ce at low temperatures (Hellman et al. 1979) and to changing oxidation conditions at shallow depth over the redox boundary (Neal and Taylor 1989; Planavsky et al. 2009) and the substitution of Ce by Fe in both goethite and hematite under oxidation and reduction environmental conditions (Fulignati et al. 1999; Planavsky et al. 2009; Zhou et al. 2013; Külah et al. 2014).

The local increase of S phases and associated Ca and K+Fe favored the formation of gypsum/anhydrite and jarosite in the clay deposit (Mutlu et al. 2006; Ece and Schroeder 2007; Sayın 2007; Ece et al. 2008). The gypsum/anhydrite and jarosite were formed possibly as a result of the alteration of pyrite within a sulfide-sulfate reducing environment (Lerouge et al. 2006; Georgieva and Velinova 2012; Kadir and Erkoyun 2012; Sayın 2016). The association of kaolinite with accessory jarosite is possibly related to the environment created by the acidic hydrothermal solutions (pH: 4–5) near the Yarıkçı spring/spa similar to those reported for Puna, Argentina, Sb epithermal veins (Dutrizac and Jambor 2000), the hydrothermal alteration in the volcanogenic massive sulfide deposit of the Black Sea region (Çelik Karakaya et al. 2012), and the hydrothermal mineral deposits of Yellowstone National Park (Bhattacharya et al. 2016). The large REE (La+Ce) values of the hydrothermal alteration systems of the Yarıkçı clay deposit depend on pH (≤2) and associated oxidized Fe and S phases (jarosite and goethite, etc.); in contrast, smaller REE (La+Ce) values occur in neutral-alkaline (pH ≥ 5.5) systems similar to that in the Uzon-Geyzernaya hydrothermal spring system, in Kamchatka, Russia (Karpov et al. 2018).

CONCLUSIONS

Field observations and mineralogical and geochemical determinations revealed that the Yarıkçı clay deposit developed by hydrothermal alteration of Mesozoic chlorite-, muscovite-, chlorite-muscovite-schist, and garnet-graphite phyllite-type parent rocks along NW–SE- and N–S-trending faults. The alteration of the parent rocks resulted in mineralogical zonation with an abundance of kaolinite in the lower part of the deposit, and smectite+kaolinite together with smectite dominating in the upper part of the deposit, and covered by a silica cap. The occurrence of Fe (oxyhydr)oxides and cristobalite/tridymite/quartz filling subvertical fractures, veins, and stockworks within the clay deposit around the faults is also an important clue to hydrothermal alteration. The occurrence of book-like kaolinite at the edge of book-like muscovite crystals revealed that alteration of muscovite within schists which show cataclastic texture favored the formation of authigenic kaolinite based on a dissolution-precipitation mechanism under acidic conditions. The association of kaolinite with star- and disc-shaped goethite and hematite, and gypsum crystals is related to acidic hydrothermal conditions. Because of the following factors:

(1) small amounts of Sr, Rb, Ba, and Zr in claystone samples (kaolinite + smectite + cristobalite/tridymite + goethite/hematite) compared with those of metamorphic host units (muscovite + chlorite + feldspar);

(2) positive correlation between Zr/Co and Zr/Ni;

(3) local enrichment of SiO_2, Fe_2O_3, S, Cu, and Au; and

(4) an increase in the LREE/(MREE+HREE) ratio, and negative Eu and Ce anomalies, the hydrothermal alteration of muscovite, garnet, plagioclase, K-feldspar, and pyroxene, within the parent rocks, supplied Al±Fe and that leaching of alkalis favored the formation of kaolinite and Al+Mg+Fe+alkalis for smectite/illite under acidic and basic conditions, respectively. The leached Si favored formation of cristobalite/tridymite/quartz either as vein/stockwork/fracture infill or as a silica cap at the top of the deposit.

ACKNOWLEDGMENTS

The authors are much indebted to anonymous reviewers for their extremely careful and constructive reviews which improved the quality of the paper significantly. The authors are also extremely grateful to the Associate Editor, Prakash B. Malla, Editor-in-Chief, Joseph W. Stucki, and Managing Editor, Kevin Murphy, for their insightful editorial comments and suggestions. This paper was presented at the 9th Mid-European Clay Conference, 2018, in Zagreb, Croatia.

Compliance with Ethical Statements

Conflict of Interest

The authors declare that they have no conflict of interest.

REFERENCES

Acarlioğlu, S., Kadir, S., Abdioğlu, E., & Arslan, M. (2013). Epithermal-alteration geology, mineralogy and geochemistry of Eocene volcanic rocks in the Hasandağ (Giresun) area, eastern Pontides, NE Turkey. *Neues Jahrbuch für Mineralogie Abhandlungen, 190*, 79–99.

Akbulut, M., Pişkin, Ö., & Karayiğit, A. İ. (2006). The genesis of the carbonatized and silicified ultramafics known as listvenites: a case study from the Mihallıççık region (Eskişehir), NW Turkey. *Geological Journal, 41*, 557–580.

Aliyari, F., Rastad, E., Goldfarb, R. J., & Sharif, J. A. (2014). Geochemistry of hydrothermal alteration at the Qolqoleh gold deposit, northern Sanandaj–Sirjan metamorphic belt, northwestern Iran: Vectors to high-grade ore bodies. *Journal of Geochemical Exploration, 140*, 111–125.

Aydınçakır, E., & Şen, C. (2013). Petrogenesis of the post-collisional volcanic rocks from the Borçka (Artvin) area: Implications for the evolution of the Eocene magmatism in the Eastern Pontides (NE Turkey). *Lithos, 172–173*, 98–117.

Barrett, T.J. & MacLean, W.H. (1994). Chemostratigraphy and hydrothermal alteration in exploration for VHMS deposits in greenstones and younger volcanic rocks. Pp. 433–467 in: *Alteration and alteration processes associated with ore-forming systems*. (D.R. Lentz,

https://doi.org/10.1007/s42860-020-00097-3 Published online by Cambridge University Press

editor). Geological Association of Canada Short Course Notes 11, NL, St Johns, Nova Scotia, Canada.
Barrett, T. J., & MacLean, W. H. (1999). Volcanic sequences, lithogeochemistry, and hydrothermal alteration in some bimodal volcanic-associated massive sulfide systems. *Reviews in Economic Geology, 8*, 101–131.
Bau, M., & Dulski, P. (1996). Distribution of yttrium and rare–earth elements in the Penge and Kuruman iron-Formations, Transvaal Supergroup, South Africa. *Precambrian Research, 79*, 37–55.
Bea, F., Montero, P., & Ortega, M. (2006). A LA–ICP–MS evaluation of Zr reservoirs in common crustal rocks: Implications for Zr and Hf geochemistry, and zircon-forming processes. *The Canadian Mineralogist, 44*, 693–714.
Bhattacharya, S., Mitra, S., Gupta, S., Jain, N., Chauhan, P., Parthasarathy, G., & Ajai. (2016). Jarosite occurrence in the Deccan Volcanic Province of Kachchh, western India: Spectroscopic studies on a Martian analog locality. *Journal of Geophysical Research: Planets, 121*, 402–431.
Boulais, P., Valley, J. M., Choux, J. E., Fourcade, S., & Martineau, F. (2000). Origin of kaolinization in Brittany (NW France) with emphasis on deposits over granite: stable isotopes (O, H) constraints. *Chemical Geology, 168*, 211–223.
Boyraz, S. (2004). Mülk-Demirci yöresi (Eskişehir-Sivrihisar) Neojen (Üst Miyosen-Pliyosen) birimlerinin kil mineralojisi. Ankara Üniversitesi, Fen Bilimleri Ensitüsü, Yüksek Lisans Tezi, Ankara (Unpublished).
Brindley, G.W. (1980). Quantitative X-ray analysis of clays. Pp. 411–438 in: *Crystal Structures of Clay Minerals and their X-ray Identification* (G.W. Brindley and G. Brown, editors). Mineralogical Society Monograph *5*, London.
Çelik Karakaya, M., Karakaya, N., Küpeli, Ş., & Yavuz, F. (2012). Mineralogy and geochemical behavior of trace elements of hydrothermal alteration types in the volcanogenic massive sulfide deposits, NE Turkey. *Ore Geology Reviews, 48*, 197–224.
Chen, C., Barcellos, D., Richter, D. D., Schroeder, P. A., & Thompson, A. (2018). Redoximorphic Bt horizons of the Calhoun CZO soils exhibit depth-dependent iron-oxide crystallinity. *Journal of Soils and Sediments, 19*, 785–797.
Craw, D., Upton, P., & Mackenzie, D. J. (2009). Hydrothermal alteration styles in ancient and modern orogenic gold deposits, New Zealand. *New Zealand Journal of Geology and Geophysics, 52*, 11–26.
Davis, P. B., & Whitney, D. L. (2006). Petrogenesis of lawsonite and epidote eclogite and blueschist, Sivrihisar Massif, Turkey. *Journal of Metamorphic Geology, 24*, 823–849.
Degeling, H., Eggins, S., & Ellis, D. J. (2001). Zr budgets for metamorphic reactions, and the formation of zircon from garnet breakdown. *Mineralogical Magazine, 65*, 749–758.
Dill, H. G., Bosse, H.-R., Henning, K.-H., Fricke, A., & Ahrendt, H. (1997). Mineralogical and chemical variations in hypogene and supergene kaolin deposits in a mobile fold belt of the Central Andes of northwestern Peru. *Mineralium Deposita, 32*, 149–163.
Dutrizac, J. E., & Jambor, J. L. (2000). Jarosites and their application in hydrometallurgy. C. N. Alpers, J. L. Jambor, & D. K. Nordstrom (Eds.), *Sulfate minerals - crystallography, geochemistry, and environmental significance* (pp. 405–452). Reviews in Mineralogy, 40. chantilly: Mineralogical Society of America.
Ece, Ö. I., & Schroeder, P. A. (2007). Clay mineralogy and chemistry of halloysite and alunite deposits in the Turplu area, Balikesir, Turkey. *Clays and Clay Minerals, 55*, 18–35.
Ece, Ö. I., Schroeder, P. A., Smilley, M. J., & Wampler, J. M. (2008). Acid-sulphate alteration of andesitic tuffs and genesis of halloysite and alunite deposits in the Biga Peninsula, Turkey. *Clay Minerals, 43*, 281–315.
Eren, M., & Kadir, S. (2013). Colour origin of red sandstone beds within the Hüdai Formation (Early Cambrian), Aydıncık (Mersin), southern Turkey. *Turkish Journal of Earth Sciences, 22*, 563–573.
Eren, M., Kadir, S., Kapur, S., Huggett, J., & Zucca, C. (2015). Colour origin of Tortonian red mudstones within the Mersin area, southern Turkey. *Sedimentary Geology, 318*, 10–19.
Erhenberg, S. N. (1991). Kaolinized, potassium-leached zones at the contacts of the Garn Formation, Haltenbanken, mid-Norwegian continental shelf. *Marine and Petroleum Geology, 8*, 250–269.
Erkoyun, H., & Kadir, S. (2011). Mineralogy, micromorphology, geochemistry and genesis of a hydrothermal kaolinite deposit and altered Miocene host volcanites in the Hallaçlar area, Uşak, western Turkey. *Clay Minerals, 46*, 421–448.
Exley, C. S. (1976). Observations on the formation of kaolinite in the St. Austell Granite, Cornwall. *Clay Minerals, 11*, 51–63.
Fraser, G., Ellis, D., & Eggins, S. (1997). Zirconium abundance in granulite-facies minerals, with implications for zircon geochronology in high-grade rocks. *Geology, 25*, 607–610.
Fujii, N., Kayabalı, İ., & Saka, A.H. (1995). *Data Book of Ceramic Raw Materials of Selected Areas in Turkey*. Monography Series No.1, General Directorate of Mineral Research and Exploration, 144 p.
Fulignati, P., Gioncada, A., & Sbrana, A. (1999). Rare-earth element (REE) behaviour in the alteration facies of the active magmatic-hydrothermal system of Vulcano (Aeolian Islands, Italy). *Journal of Volcanology and Geothermal Research, 88*, 325–342.
Georgieva, S., & Velinova, N. (2012). Alunite from the advanced argillic alterations in the Chelopech high sulphidation epithermal Cu-Au deposit, Bulgaria: Chemistry, morphology and genetic significance. *Bulletin of Mineralogy Petrology and Geochemistry, 49*, 17–31.
Ghanem, H., & Jarrar, G. H. (2013). Geochemistry and petrogenesis of the 595 Ma shoshonitic Qunai monzogabbro, Jordan. *Journal of African Earth Sciences, 88*, 1–14.
Gifkins, C., Herrmann, W., & Large, R. (2005). *Altered volcanic rocks: A guide to description and interpretation: Australia*. Centre for Ore Deposits and Exploration Studies, University of Tasmania, 275 pp.
Gözler, M.Z., Cevher, F., Ergül, E., & Asutay, H.J. (1996). *Orta Sakarya ve güneyinin jeolojisi*, Mineral Research and Exploration (MTA) Report No. 9973 (Unpublished).
Grant, J. A. (1986). The isocon diagram – a simple solution to Gresens' equation for metasomatic alteration. *Economic Geology, 81*, 1976–1982.
Grant, J. A. (2005). Isocon analysis: A brief review of the method and applications. *Physics and Chemistry of the Earth, 30*, 997–1004.
Gürsu, S., Göncüoglu, M. C., & Bayhan, H. (2004). Geology and geochemistry of the Pre-early Cambrian rocks in the Sandikli area: implications for the Pan-African evolution NW Gondwanaland. *Gondwana Research, 7*, 923–935.
Haines, S. H., & van der Pluijm, B. A. (2012). Patterns of mineral transformations in clay gouge, with examples from low-angle normal fault rocks in the western USA. *Journal of Structural Geology, 43*, 2–32.
Harnois, L. (1988). The CIW index: A new chemical index of weathering. *Sedimentary Geology, 55*, 319–322.
Hellman, P. L., Smith, R. E., & Henderson, P. (1979). Rare element investigation of the Cliefden outcrop, N.S.W., Australia. *Contributions to Mineralogy and Petrology, 65*, 155–164.
Inoue, A. (1995). Formation of clay minerals in hydrothermal environments. Pp. 268–329 in: *Origin and Mineralogy of Clays: Clays and the Environment* (B. Velde, editor). Springer, Berlin, Heidelberg.
Jele, N.L. (2013). *The genesis of the quartz-sericite schists of the Toggekry Formation, Nondweni greenstone Belt, South Africa. School of Agricultural, Earth and Environmental Sciences*, MSc thesis, University of KwaZulu-Natal, Durban, 159 pp.
Kadir, S., & Akbulut, A. (2009). Mineralogy, geochemistry and genesis of the Taşoluk kaolinite deposits in pre-Early Cambrian metamorphites and Neogene volcanites of Afyonkarahisar, Turkey. *Clay Minerals, 44*, 89–112.
Kadir, S., & Erkoyun, H. (2012). Genesis of the hydrothermal Karaçayır kaolinite deposit in Miocene volcanics and Palaeozoic metamorphic rocks of the Uşak-Güre basin, Western Turkey. *Turkish Journal of Earth Sciences, 21*, 1–26.
Kadir, S., & Erkoyun, H. (2015). Characterization and distribution of fibrous tremolite and chrysotile minerals in the Eskişehir region of western Turkey. *Clay Minerals, 50*, 441–458.

Kadir, S., Erman, H., & Erkoyun, H. (2011). Mineralogical and geochemical characteristics and genesis of hydrothermal kaolinite deposits within Neogene volcanites, Kütahya (western Anatolia), Turkey. *Clays and Clay Minerals, 59*, 250–276.

Kadir, S., Külah, T., Eren, M., Önalgil, N., & Gürel, A. (2014). Mineralogical and geochemical characteristics and genesis of the Güzelyurt alunite–bearing kaolinite deposit within the Late Miocene Gördeles ignimbrite, central Anatolia, Turkey. *Clays and Clay Minerals, 62*, 477–499.

Kadir, S., Aydoğan, M. S., Elitok, Ö., & Helvacı, C. (2015). Composition and genesis of the nickel-chrome-bearing nontronite and montmorillonite in lateritized ultramafic rocks in the Muratdağı region (Uşak, western Anatolia), Turkey. *Clays and Clay Minerals, 63*, 163–184.

Kadir, S., Eren, M., İrkeç, T., Erkoyun, H., Külah, T., Önalgil, N., & Huggett, J. (2017). An approach to genesis of sepiolite and palygorskite in lacustrine sediments of the Lower Pliocene Sakarya and Porsuk Formations in the Sivrihisar and Yunusemre-Biçer regions (Eskişehir), Turkey. *Clays and Clay Minerals, 65*, 310–328.

Kämpf, N., Scheinost, A.C., & Schulze, D.G. (2000). Oxide Minerals. Pp. 125–168 in: *Handbook of Soil Science* (M.E. Sumner, editor). Boca Raton, Florida.

Karakaş, Z., Karakaş, Ö., & Varol, B. (2007). Sazak-Biçer (Sivrihisar KD'su) civarı Neojen (Miyosen-Pliyosen) göl basenindeki kiltaşlarının mineralojik incelemesi. *Türkiye Jeoloji Bülteni, 50*, 57–69.

Karpov, G. A., Schroeder, P. A., & Nikolaeva, A. G. (2018). Geochemistry of rare elements in thermal waters of Uzon-Geyzernaya hydrothermal system (Kamchatka). *Russian Geology and Geophyscics, 59*, 925–934.

Keller, W. D. (1976). Scan electron micrographs of kaolins collected from diverse origin-III. influence of parent material on flint clays and flint-like clays. *Clays and Clay Minerals, 24*, 262–264.

Koçak, A. (1975). *Mihalıççık Yarıkçı kaplıcası hidrojeolojik etüdü*. MTA Report No. 5818, Ankara.

Külah, T., Kadir, S., Gürel, A., Eren, M., & Önalgil, N. (2014). Mineralogy, geochemistry, and genesis of mudstones in the upper Miocene Mustafapaşa member of the Ürgüp formation in the Cappadocia region, central Anatolia, Turkey. *Clays and Clay Minerals, 62*, 267–285.

Kulaksız, S. (1981). Sivrihisar KB sının jeolojisi. *Hacettepe Üniversitesi Yerbilimleri Dergisi, 8*, 103–124.

Kunze, G.W. & Dixon, J.B. (1986). Pretreatment for mineralogical analysis. Pp. 91–100 in: *Methods of Soil Analysis, Part 1. Physical and Mineralogical Methods* (2nd edition) (A. Klute, editor). American Society of Agronomy, Inc. and the Soil Science Society of America, Inc., Madison, Wisconsin, USA.

Lee, R.G., Dilles, J.H., Mazdab, F.K., & Wooden, J.L. (2009). Europium anomalies in zircon from granodiorite porphyry intrusions at the El Salvador porphyry copper deposit, Chile. *The Geological Society of America*, paper no 158-8.

Lerouge, C., Kunov, A., Fléhoc, C., Georgieva, S., Hikov, A., Lescuyer, J. L., Petrunov, R., & Veliova, N. (2006). Constraints of stable isotopes on the origin of alunite from advanced argillic alteration systems in Bulgaria. *Journal of Geochemical Exploration, 90*, 166–182.

López-Moro, F. J. (2012). EASYGRESGRANT – A Microsoft Excel spreadsheet to quantify volume changes and to perform mass-balance modeling in metasomatic systems. *Computers and Geosciences, 39*, 191–196.

MacLean, W. H., & Barrett, T. J. (1993). Lithogeochemical techniques using immobile elements. *Journal of Geochemical Exploration, 48*, 109–133.

Maulana, A., Christy, A. G., Ellis, D. J., & Bröcker, M. (2019). The distinctive tectonic and metamorphic history of the Barru Block, South Sulawesi, Indonesia: Petrological, geochemical and geochronological evidence. *Journal of Asian Earth Sciences, 172*, 170–189.

McFarlane, C. R. M., Mavrogenes, J. A., & Tomkins, A. G. (2007). Recognizing hydrothermal alteration through a granulite facies metamorphic overprint at the challenger Au deposit, South Australia. *Chemical Geology, 243*, 64–89.

Meunier, A. (1995). Hydrothermal alteration by veins. In B. Velde (Ed.), *Origin and mineralogy of clays: clays and the environment* (pp. 247–267). Berlin: Springer-Verlag.

Meunier, A. (2005). *Clays*. Berlin, Heidelberg: Springer Verlag.

Meunier, A., & Velde, B. (2004). *Illite, Origin, Evolution and Metamorphism. Springer-Verlag* (p. 286). Berlin, Heidelberg: New York.

Mongelli, G. (1997). Ce-anomalies in the textural components of Upper Cretaceous karst bauxites from the Apulian carbonate platform (southern Italy). *Chemical Geology, 140*, 69–79.

Moore, D. M., & Reynolds, R. C. (1989). *X-ray Diffraction and the Identification and Analysis of Clay Minerals*. New York: Oxford University Press.

Mutlu, H., Sarıız, K., & Kadir, S. (2006). Geochemistry and origin of the Şaphane alunite deposit, western Anatolia, Turkey. *Ore Geology Review, 26*, 39–50.

Nagasawa, K. (1978). Kaolin minerals. Pp. 189–219 in: *Clays and Clay Minerals of Japan* (T. Sudo and S. Shimoda, editors). Developments in Sedimentology, *26*, Elsevier, Tokyo.

Neal, C. R., & Taylor, L. A. (1989). A negative Ce anomaly in a peridotite xenolith: Evidence for crustal recycling into the mantle or mantle metasomatism? *Geochimica et Cosmochimica Acta, 53*, 1035–1040.

Okay, A. I. (1989). Alpine-Himalayan blueschists. *Annual Reviews of the Earth and Planetary Sciences, 17*, 55–87.

Okay, A. I., Tansel, İ., & Tüysüz, O. (2001). Obduction, subduction and collision as reflected in the Upper Cretaceous–Lower Eocene sedimentary record of western Turkey. *Geological Magazine, 138*, 117–142.

Ömeroğlu Sayıt, I., Günal Türkmenoğlu, A., Sayın, Ş. A., & Demirci, C. (2018). Hydrothermal alteration products in the vicinity of the Ahırözü kaolin deposits, Mihalıççık-Eskişehir, Turkey. *Clay Minerals, 53*, 289–303.

Parry, W. T., Ballantyne, J. M., & Jacobs, D. C. (1984). Geochemistry of hydrothermal sericite from Roosevelt hot springs and the Tintic and Santa Rita porphyry copper systems. *Economic Geology, 79*, 72–86.

Planavsky, N., Rouxel, O., Bekker, A., Shapiro, R., Fralick, P., & Knudsen, A. (2009). Iron-oxidizing microbial ecosystems thrived in late Paleoproterozoic redox-stratified oceans. *Earth and Planetary Science Letters, 286*, 230–242.

Santamarina, J.C., Klein, K.A., Palomino, A., & Guimaraes, M.S. (2002). Micro-scale aspects of chemical-mechanical coupling – interparticle forces and fabric. Pp. 47–64 in: *Chemical Behaviour: Chemo-Mechanical Coupling from nano-Structure to Engineering Applications* (C. Di Maio, T. Hueckel, and B. Loret, editors). Maratea, Balkema, Rotterdam, The Netherlands.

Sayın, S. A. (2007). Origin of kaolin deposits: Evidence from the Hisarcık (Emet-Kütahya) deposits, western Turkey. *Turkish Journal of Earth Sciences, 16*, 77–96.

Sayın, Ş. A. (2016). Quartz-mica schist and gneiss hosted clay deposits within the Yenipazar (Yozgat, Central Anatolia) volcanogenic massive sulfide ore. *Turkish Journal of Earth Sciences, 25*, 81–101.

Schwertmann, U. (1993). Relation between iron oxides, soil color, and soil formation. Pp. 51–69 in: *Soil Color* (J.M. Bigham and E.J. Ciolkosz, editors). Soil Science Society of America, Madison, Wisconsin, USA.

Şengör, A. M. C., & Yılmaz, Y. (1981). Tethyan evolution of Turkey: a plate tectonic approach. *Tectonophysics, 75*, 181–241.

Şengör, A.M.C., Görür, N., & Şaroglu, F. (1985). Strike-slip faulting and related basin formation in zones of tectonic escape: Turkey as a case study. Pp. 227–264 in: *Strike-Slip Deformation, Basin Formation and Sedimentation* (K.T. Biddle, & N. Christie-Blick, editors). Society of Economic Paleontologists and Mineralogists (SEPM) Special Publication, 37.

Serna, E. (2014). Geochemistry and Genesis of Late Paleoproterozoic Banded Iron Formations and Metamorphosed Chemical Precipitates Spatially Associated with Pb-Zn Broken Hill-type Mineralization

near the Broken Hill Deposit, Curnamona Province, Australia. Faculty of the Department of Geological Sciences Thomas Harriot College of Arts and Sciences, MSc thesis, East Carolina University, 113p.

Seyhan, İ. (1968). *Mihalıççık (Eskişehir) Ahıröz ü-Üçbaşlı ve Sazak kaolenleri hakkında rapor*. MTA Rapor No. 3922, 40s, Ankara.

Seyhan, İ. (1978). Türkiye kaolin yatakları ve hidrotermal cevherler arasında görülen ilişkiler. *Jeoloji Mühendisliği Dergisi, 4*, 27–31 Ankara.

Spry, P. G., Adriana, H., Messerly, J. D., & Houk, R. S. (2007). Discrimination of metamorphic and metasomatic processes at the Broken Hill Pb-Zn-Ag deposit, Australia: rare element signatures of garnet-rich rocks. *Economic Geology, 102*, 471–494.

State Planning Organization of Turkey (2001). 8th Five-Year Development Plan, Mining Special Expert Commission Report, Volume 1, Industrial Sub-Commission Ceramic clays-Kaolin-Pyrophyllite-Wollastonite-Talc Group, Ankara, 224 pp. (http://ekutup.dpt.gov.tr/madencil/sanayiha/oik622.pdf)

Sverjensky, D. A. (1982). Europium equilibria in aqueous solution. *Earth and Planetary Science Letters, 67*, 70–78.

Taillefer, A., Soliva, R., Guillou-Frottier, L., Le Goff, E., Martin, G., & Seranne, M. (2017). Fault-related controls on upward hydrothermal flow: An integrated geological study of the Têt Fault System, Eastern Pyrénées (France). *Geofluids, 2017*, 1–19.

Taylor, S. R., & McLennan, S. M. (1985). *The Continental Crust: Its Composition and Evolution*. Oxford, UK: Blackwell 312 pp.

Velde, B. (1985). Clay minerals: A Physico-chemical explanation of their occurrence. *Development of Sedimentology*, *40*, Elsevier, New York, 427 pp.

Vidal, P. (1998). *Géochimie.* Série geosciences. Dunod, Paris.

Wang, W., Tang, J., Xu, W.-L., & Wang, F. (2015). Geochronology and geochemistry of Early Jurassic volcanic rocks in the Erguna Massif, northeast China: Petrogenesis and implications for the tectonic evolution of the Mongol–Okhotsk suture belt. *Lithos, 218-219*, 73–86.

Whitney, D. L., & Evans, B. W. (2010). Abbreviations for names of rock-forming minerals. *American Mineralogist, 95*, 185–187.

Wilson, M. J. (1987). *A Handbook of Determinative Methods in Clay Mineralogy*. New York: Blackie and Son.

Yalçın, H., & Bozkaya, Ö. (2003). Sivas batısındaki (Yıldızeli-Akdağ madeni) hidrotermal kaolinite ve I-S oluşumlarının mineralojisi ve jeokimyası. *Türkiye Jeoloji Bülteni, 46*, 1–23.

Yılmaz, Y. (1981). Sakarya kıtası güney kenarının tektonik evrimi. *Yerbilimleri, 1*, 33–52.

Yılmaz, Y., Genc, Ş. C., Gürer F., Bozcu, M., Yılmaz, K., Karacık, Z., Altunkaynak, Ş, & Elmas, A. (2000). When did the western Anatolian grabens begin to develop? Pp. 353–384 in: *Tectonics and Magmatism in Turkey and the Surrounding Area* (E. Bozkurt, J.A. Winchester, and J.D.A Piper, editors). Special Publications *173*, Geological Society, London.

Zhou, L., Zhang, Z., Li, Y., You, F., Wu, C., & Zheng, C. (2013). Geological and geochemical characteristics in the paleo-weathering crust sedimentary type REE deposits, western Guizhou, China. *Journal of Asian Earth Sciences, 73*, 184–198.

(Received 4 May 2020; Revised 5 August 2020; AE: Prakash B. Malla)